Available online at www.sciencedirect.com
ScienceDirect
Geochimica et Cosmochimica Acta 71 (2007) 4668–4692
Geochimica et Cosmochimica Acta
www.elsevier.com/locate/gca

Sulfur and carbon isotope records from 1700 to 800 Ma carbonates of the Jixian section, northern China: Implications for secular isotope variations in Proterozoic seawater and relationships to global supercontinental events

Xuelei Chu [a,b,*], Tonggang Zhang [a,b], Qirui Zhang [a], Timothy W. Lyons [c]

[a] *Institute of Geology and Geophysics, Chinese Academy of Sciences, P.O. Box 9825, Beijing 100029, China*
[b] *Key Laboratory for Mineral Resources, Chinese Academy of Sciences, Beijing 100029, China*
[c] *Department of Earth Sciences, University of California, Riverside, CA 92521, USA*

Received 2 October 2006; accepted in revised form 17 July 2007; available online 14 August 2007

Abstract

This study is a comprehensive, stable isotope survey of the marine carbonate-dominated, upper Paleo- to lower Neoproterozoic stratigraphy of Jixian County, China. Carbonate-associated sulfate (CAS) was extracted and measured for $\delta^{34}S_{CAS}$ using the same samples analyzed for $\delta^{13}C_{carbonate}$. This integrated proxy approach is a step towards a more comprehensive picture of secular variation in the composition of Proterozoic seawater. We specifically sampled marine carbonate intervals from the lower section of the Chuanlinggou Formation, Changcheng Group (ca. 1700 Ma) to the top of the Jingeryu Formation, Qingbaikou Group (ca. 800 Ma). $\delta^{13}C_{carbonate}$ values are mostly negative in the upper Paleoproterozoic Changcheng Group, with an ascending trend from −3‰ to 0‰. We observed variation of approximately 0 ± 1‰ in the Mesoproterozoic Jixian Group, and positive values of $+2 \pm 2$‰ characterize the lower Neoproterozoic Qingbaikou Group. Stratigraphic variations in $\delta^{34}S_{CAS}$ are more remarkable in their ranges and magnitudes, including conspicuously high values exceeding +30‰ in the three intervals at ca. 1700 Ma, 1300–1100 Ma, and 1000–900 Ma. In the Changcheng Group, $\delta^{34}S_{CAS}$ values are typically higher than +25‰, with only a few values of less than +15‰. In contrast, most of the data spanning from the Mesoproterozoic Tieling Formation of the Jixian Group to the lower Neoproterozoic Jingeryu Formation of the Qingbaikou Group are highly variable between +10‰ and +25‰, with some values exceeding +25‰.

In the late Paleoproterozoic (1700–1600 Ma), a >10‰ decrease in $\delta^{34}S_{CAS}$ and ~3‰ increase in $\delta^{13}C_{carbonate}$ are coincident with, and likely related to, the breakup of Columbia, a supercontinent that predated Rodinia. Carbon and sulfur isotope data from the Mesoproterozoic, when global tectonic activity was comparatively weaker, fall mostly in the ranges of $+15 \pm 10$‰ and 0 ± 1‰, respectively, but fluctuations of >20‰ for $\delta^{34}S_{CAS}$ and >3‰ for the $\delta^{13}C_{carbonate}$ at ca. 1450–1400 Ma may reflect subduction and large-scale magmatic activity in island arcs marking the end of Columbia breakup. From the late Mesoproterozoic (ca. 1300–1100 Ma) to the early Neoproterozoic (ca. 800 Ma), the $\delta^{13}C$ and $\delta^{34}S$ of seawater increased gradually with increasing variability. Most impressive are $\delta^{34}S_{CAS}$ values that exceed +30‰ in two intervals at ca. 1300–1100 Ma and ca. 1000–900 Ma, which may reflect the assembly and early breakup of Rodinia. Although gaps in the record remain, and studies of even higher resolution are warranted, our results suggest that changes in paleoceanographic conditions linked to global tectonics strongly influenced the biogeochemical cycles of C and S. Furthermore, periods of the Proterozoic previously noted for their isotopic invariability show clear isotopic expressions of this tectonic activity.

* Corresponding author. Fax: +86 10 62010846.
E-mail address: xlchu@mail.iggcas.ac.cn (X. Chu).

0016-7037/$ - see front matter © 2007 Elsevier Ltd. All rights reserved.
doi:10.1016/j.gca.2007.07.017

1. INTRODUCTION

Models for tectonic, chemical, and biological change during the Precambrian commonly rely on historic variations in the stable isotopic compositions of marine sedimentary rocks (e.g., Shields and Veizer, 2002; Lindsay and Brasier, 2002; Bartley and Kah, 2004). Sulfur and carbon isotopes have been used widely to explore changes in biogeochemical cycling linked to tectonic events, biological innovations, and changes in the oxidation state of Earth's surface (Schidlowski et al., 1975; Des Marais et al., 1992; Canfield and Teske, 1996; Farquhar et al., 2000; Godderis and Veizer, 2000; Hurtgen et al., 2002; Johnston et al., 2005). In addition to evolutionary questions, S and C data can also be used for stratigraphic correlations. This is particularly important for the Precambrian, which lacks a robust biostratigraphic framework (Walter et al., 2000). Consequently, isotopic approaches are used often in Precambrian research (Kaufman and Knoll, 1995; Brasier et al., 1996; Kaufman et al., 1997; Gorjan et al., 2000; Walter et al., 2000; Shields et al., 2004).

Previous studies have focused mostly on two time intervals, the middle Archean to middle Paleoproterozic (3500–1900 Ma) and the late Neoproterozoic (800–544 Ma) (e.g., Gorjan et al., 2000; Bartley et al., 2001; Lindsay and Brasier, 2002; Ray et al., 2003). This emphasis reflects the former interval's connection to the early oxygenation of the atmosphere and ocean and associated evolution of the biosphere (Kasting, 1987; Karhu and Holland, 1996; Des Marais, 1997), while the latter provides us with an exceptional, globally distributed record of "snowball Earth" conditions (Hoffman et al., 1998). Correspondingly, the Precambrian secular curve for $\delta^{13}C_{carbonate}$ is known to be bimodal, with major, well defined oscillatory peaks at ca. 2300–2200 Ma, immediately following the so-called Great Oxidation Event (Holland, 2002; Bekker et al., 2004), and at ca. 650 Ma (Lindsay and Brasier, 2004), marking the time of widespread Neoproterozoic glaciation (Fig. 1). The time interval of 1900–800 Ma has received less attention due to its relatively flat curve for $\delta^{13}C_{carbonate}$ (Fig. 1), which led Buick et al. (1995) to dub the Mesoproterozoic as "the dullest time in Earth history".

Growing geological and biogeochemical evidence suggests, however, that the Mesoproterozoic may have been a time of significant global tectonic reorganization, marked by the breakup of the supercontinent Columbia and subsequent assembly of Rodinia, and evolutionary diversification in both prokaryotic and eukaryotic communities (Hoffman, 1991; Kah and Bartley, 2001; Zhao et al., 2002, 2004; Lindsay and Brasier, 2004; Bartley and Kah, 2004; Lyons et al., 2004a). Significant excursions in $\delta^{34}S_{sulfate}$ and/or $\delta^{13}C_{carbonate}$ can be used to document major tectonic and biogeochemical events in Earth history (e.g., Des Marais et al., 1992; Kaufman and Knoll, 1995; Strauss, 1999; Frank

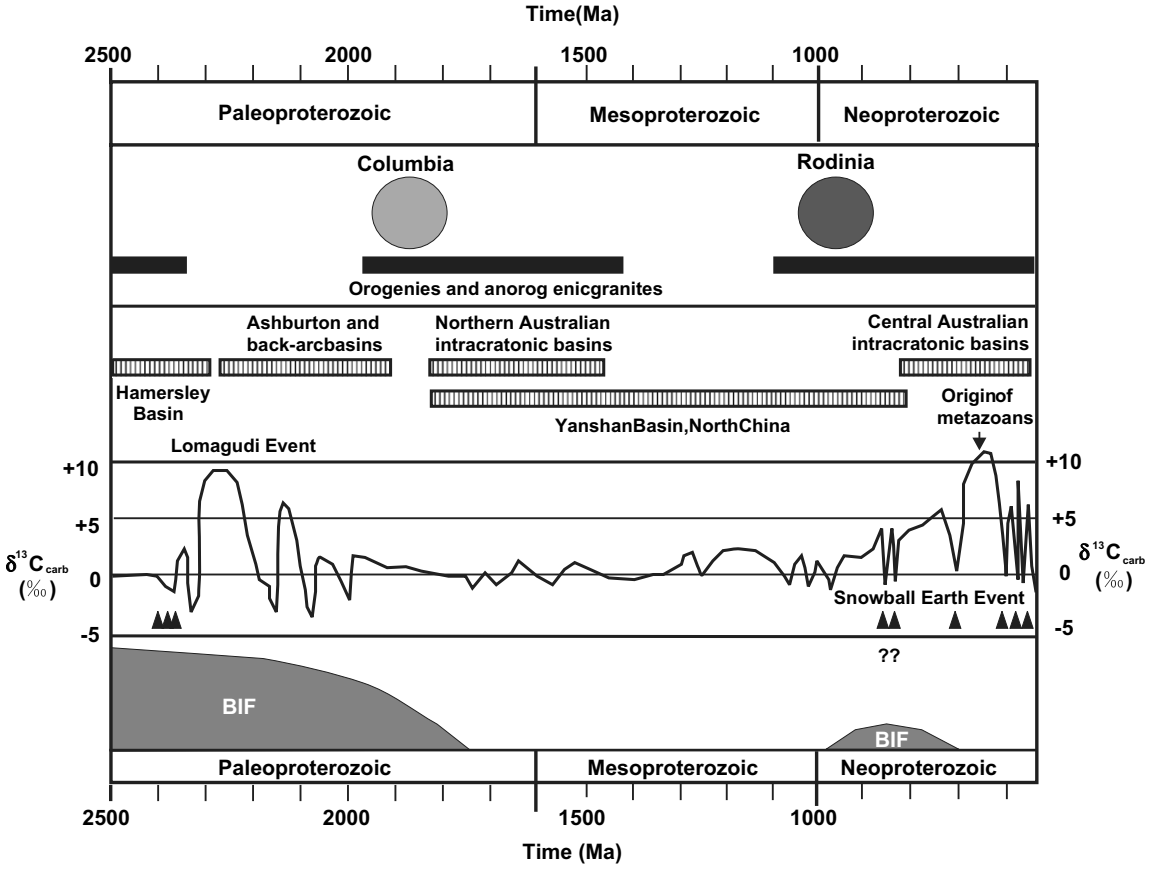

Fig. 1. Outline of carbon isotope, tectonic, and biospheric changes through the Proterozoic. After Figs. 5.3-6 of Lindsay and Brasier (2004). (Circles) Supercontinents; (black bars) supercontinent events; (hachured bars) intracratonic basins; (black triangles) glaciations.

et al., 2003; Lindsay and Brasier, 2004; Bartley and Kah, 2004; Lyons et al., 2004a). Previously published data suggest that $\delta^{13}C_{carbonate}$ values lie within a relatively narrow range of about $+1.5 \pm 0.5‰$ during the Mesoproterozoic (Buick et al., 1995; Knoll et al., 1995) and $+0.6 \pm 1‰$ for the transition from the Paleoproterozoic to Mesoproterozoic (Brasier and Lindsay, 1998; Lindsay and Brasier, 2000) and show comparatively little variation in the interval from ca. 1800 to 1000 Ma (Kaufman et al., 1997; Lindsay and Brasier, 2004). In contrast, our data suggest a more complex fabric of isotopic variation for the Proterozoic.

Historically, Proterozoic sulfate–sulfur isotope data have been insufficient for building a reliable secular isotope curve because of the lack of Precambrian evaporites (Claypool et al., 1980; Strauss, 1993). As an alternative to gypsum and anhydrite, carbonate-associated sulfate (CAS) is improving the continuity of sulfur isotope records of contemporaneous seawater sulfate for this interval (Strauss, 1993; Hurtgen et al., 2002; Kampschulte and Strauss, 2004; Kah et al., 2004; Lyons et al., 2004a; Gellatly and Lyons, 2005). To date, however, only limited data for CAS have been published, and there are still few results from carbonate successions spanning the Mesoproterozoic.

In this paper we explore well preserved strata of the Jixian section in northern China, which are believed to span a large portion of the Proterozoic Era from ca. 1800 to 800 Ma with relatively few major interruptions (Kao et al., 1934; Chen et al., 1980; Jahn and Cuvellier, 1994; Lu et al., 1996; Xiao et al., 1997; Li et al., 2003a). Because of the section's high quality—including a thickness exceeding 9000 m, relatively continuous deposition, and well preserved sedimentary features—the section was considered for the international stratotype of the Middle-to-Late Proterozoic (Wang and Qiao, 1987; Jahn and Cuvellier, 1994; Lu et al., 1996). Studies of the section's sedimentology, stratigraphy, paleontology, geochronology, and isotope and organic geochemistry have been published previously (Chen et al., 1980; Hofmann and Chen, 1981; Jahn and Cuvellier, 1994; Zhu and Chen, 1995; Lu et al., 1996; Seong-Joo and Golubic, 1999; Xiao et al., 1997; Zhu et al., 2000; Li et al., 2003a; Chu et al., 2004). These data provide an ideal backdrop for our investigation of sulfur and carbon isotope

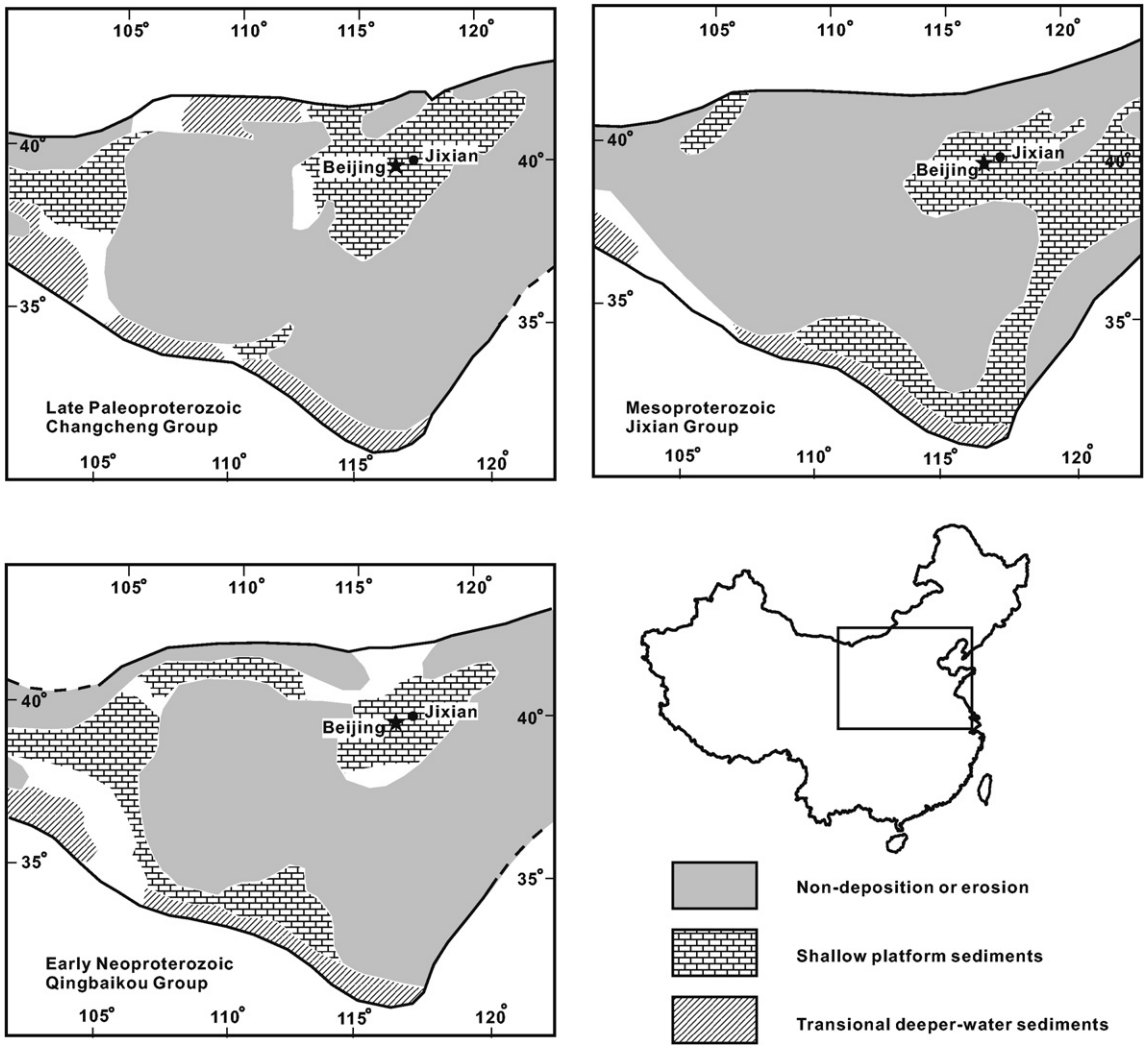

Fig. 2. Simplified late Paleo-, Meso-, and early Neoproterozoic paleogeographic maps of the North China Craton. Modified from Wang (1985) and Li et al. (2003b). All samples were collected from the Jixian County.

variations at a resolution suitable for global-scale chemostratigraphic comparisons. Carbon isotope variations in the Jixian section were reported previously without data tables in a Chinese journal (Chu et al., 2004). Here, we present these carbon isotope data for the major carbonate formations of the Jixian section in light of a new and exhaustive set of sulfur isotope results. As a proxy for seawater sulfate, CAS can be extracted and measured for $\delta^{34}S_{sulfate}$ using splits from the same samples employed in $\delta^{13}C_{carbonate}$ analysis. This comprehensive exploration of secular variations in $\delta^{34}S$ and $\delta^{13}C$ for Proterozoic seawater as recorded in the Jixian section should provide an important foundation for future investigations performed at even higher resolution. As such, this study takes us one significant step closer to the global isotope curves that are still elusive for the Proterozoic.

2. GEOLOGICAL SETTING

The most complete Proterozoic stratigraphic succession in China is best exposed in the Jixian region, about 100 km east of Beijing (Fig. 2). The section is dominated by marine carbonates of several thousand meters thickness spanning much of the sedimentary history of the late Paleo-, Meso-, and early Neoproterozoic (Figs. 2 and 3). The unmetamorphosed clastic and carbonate sediments were likely deposited in a failed rift basin that extended for ~800 km along its long axis (Wang and Qiao, 1987). The Proterozoic stratigraphic section in Jixian was first described by Kao et al. (1934). Later, Chen et al. (1980) performed detailed stratigraphic, paleontologic, and sedimentologic analysis of the Jixian section and divided the ~9000 m thick succession into four groups and 11 formations. Recently, the Jixian section was divided into three groups and 12 formations (Lu et al., 1996): (1) the Changcheng, consisting of the Changzhougou, Chuanlinggou, Tuanshanzi, and Dahongyu formations; (2) the Jixian, composed of the Gaoyuzhuang, Yangzhuang, Wumishan, Hongshuizhuang, and Tieling formations; and (3) the Qingbaikou Group, consisting of the Xiamaling, Changlongshan, and Jingeryu formations (Fig. 3). Rocks of the three groups are distributed widely across the North China Craton (Fig. 2). Siliciclastic units are present, such as the Changzhougou and Chuanlinggou formations of the lower Changcheng Group and the Xiamaling and Changlongshan formations of the lower Qingbaikou Group, but marine carbonates comprise approximately 75% of the total thickness of the Jixian section (Chen et al., 1980).

2.1. Upper Paleoproterozoic Changcheng Group

In the Changcheng Group, the Chuanlinggou Formation consists dominantly of silty illitic shale with numerous sandstone lenses; the formation is subdivided into three members thought to represent the littoral–intertidal zone (Lu et al., 1996; Li et al., 2003b). The second member of the Chuanlinggou Formation is composed of black shale of subtidal to lagoonal origin with frequent intercalations of intertidal sandstone. A small amount of carbonaceous dolostone can be found in the upper part of this member; our Chuanlinggou samples were collected from this upper interval. The overlying third member consists of black shale enriched in organic carbon. Above the Chuanlinggou, the Tuanshanzi Formation is composed of muddy and silty dolomicrite with a total thickness of 528 m. We sampled dolomicrite continuously through this interval. The lower member of this formation is rich in muddy, silty, and carbonaceous rocks, which were probably deposited under slightly reducing conditions in the subtidal zone. The upper

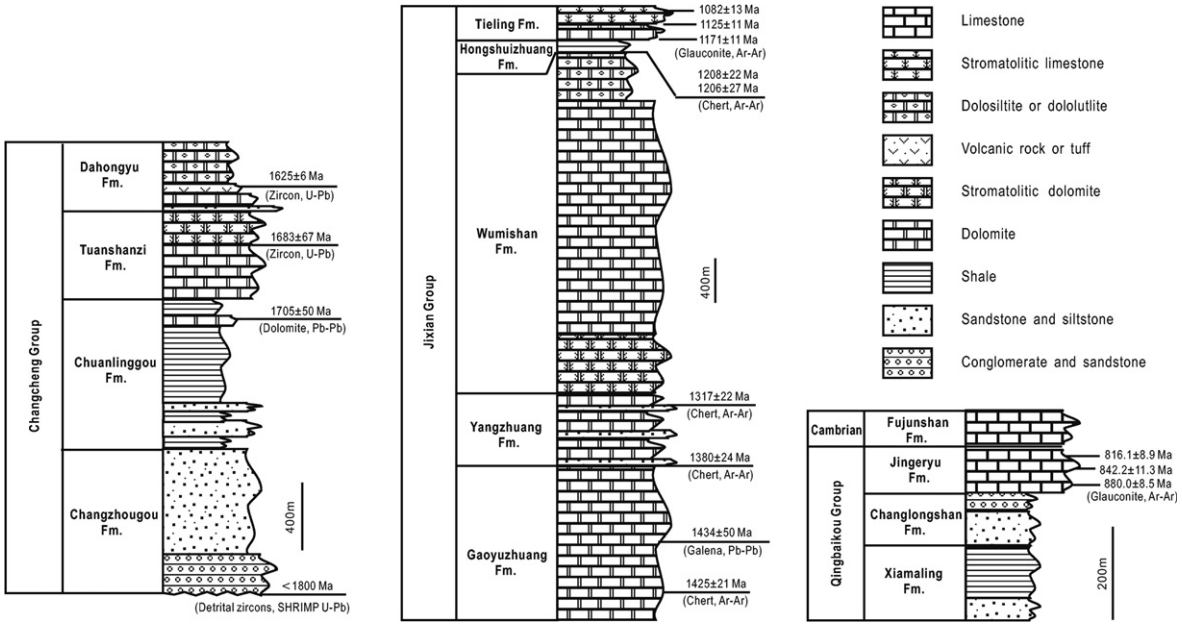

Fig. 3. Stratigraphic column with available ages for Proterozoic sedimentary successions in the Jixian section. Details are available in the text and in reference cited therein.

member was deposited in the intertidal to supratidal zone. Overlying the Tuanshanzi, the Dahongyu Formation, with a thickness of 408 m, can be subdivided into two parts (Chen et al., 1980; Lu et al., 1996): (1) a lower quartz sandstone and sandy dolostone, intercalated with volcanic tuff, tuffaceous sandstone, and high potassium lava, and (2) an upper dolomicrite and cherty dolomicrite with abundant stromatolites. Sandy dolostone and cherty dolomicrite were difficult to digest in HCl, so we have obtained only limited carbon and sulfur isotope data from the Dahongyu Formation. Contacts between the Dahongyu and the Tuanshanzi formations and between the Tuanshanzi and the Chuanlinggou formations are conformable.

2.2. Mesoproterozoic Jixian Group

The Gaoyuzhuang Formation, the lowermost portion of the Jixian Group, shows a disconformable contact with the underlying Dahongyu Formation of the Changcheng Group (Chen et al., 1980; Lu et al., 1996). The Gaoyuzhuang, with a thickness of 1588 m, is composed of dolomite and dolomitic limestone interpreted to record littoral and neritic facies and is subdivided into four members (moving up section): (1) cherty dolomicrite intercalated with clayey dolomicrite and shale; (2) thin Mn-rich dolomicrite and thick to massive dolosparite; (3) muddy dolomicrite and dolomitic micrite; and (4) bituminous dolostone, dolomitic micrite, dolosparite, and dolomicrite with cherty concretion. Above the Gaoyuzhuang, the 707 m thick Yangzhuang Formation consists of purple and white interbeds of argillite-like, silt-bearing dolomicrite and is subdivided into three members based on changes in lithofacies. The Wumishan Formation is the thickest unit in the Jixian Group, with a thickness of 3336 m. This unit is composed of four members of thickly bedded siliceous dolomite intercalated with chert bands. The lithologies of the four members are briefly described, in ascending order, as (1) alternating argillaceous, cherty, and bituminous dolomicrite or dolostone; (2) shaly dolomicrite, thick-bedded stromatolitic, and thrombolite-like dolosparite with chert layers and bituminous dolostone; (3) rhythms of silt and calcitic dolomicrite as well as oolitic dolostone with black chert layers; and (4) calcitic and cherty dolomicrite intercalated with bituminous dolostone and a bed of glauconite-bearing stromatolitic dolostone at the top. The Hongshuizhuang Formation consists of 131 m of neritic varicolored shale subdivided into two members. The lower and upper members are intercalated with thin dolomite and sandstone, respectively. The overlying Tieling Formation (333 m) is composed of two members: the lower shale member and the upper limestone member, which are separated by a ~2 m layer of discontinuous SEDEX (sedimentary exhalative) mineralization consisting of jaspilite and Mn-bearing, dolomitic limestone (Lu et al., 1996). Stromatolites are found in all the carbonates of the Jixian Group and are especially well developed in the Gaoyuzhuang, Wumishan, and Tieling formations. The Tieling Formation in the Jixian area is well known for its exceptional occurrences of stromatolites (Lu et al., 1996). We sampled continuously across the Jixian Group, which is generally interpreted to reflect sedimentation without major gaps.

2.3. Lower Neoproterozoic Qingbaikou Group

The Xiamaling Formation, the lowest unit of the Qingbaikou Group, is in disconformable contact with the underlying Tieling Formation of the Jixian Group. The Xiamaling and overlying Changlongshan formations are composed mainly of fine-grained siliciclastic rocks. The Jingeryu Formation at the upper part of the Qingbaikou Group is a ~100 m thick marine carbonate consisting of thin grayish green and light red micritic limestones of neritic to subtidal origin. Samples were collected continuously from the Jingeryu limestone.

2.4. Age Relationships

About 200 geochronological data including K–Ar, Ar–Ar, Rb–Sr, Pb–Pb, and U–Pb ages are available from Proterozoic strata in Jixian and adjacent areas (Chung, 1977; Lu et al., 1996). The most reliable of these data are cited in this paper and are shown on Fig. 3. A boundary age between the Changcheng and Jixian groups of ca. 1600 Ma (Lu et al., 1996) is estimated from a single zircon U–Pb age of 1625 ± 6 Ma from the Dahongyu volcanic rocks in the Jixian (Lu and Li, 1991). We can place the sedimentary age of dolomite in Member III of the Chuanlinggou Formation at ca. 1700 Ma based on a 1705 ± 50 Ma Pb–Pb isochron age for dolomite in the Ming Tombs section in Beijing (Jahn and Cuvellier, 1994) and a 1683 ± 67 Ma U–Pb age for authigenic zircon from K-rich trachyandesite of the Tuanshanzi Formation in Pinggu County of Beijing (Li et al., 1995). Recently, SHRIMP U–Pb dating of detrital zircons from the Changzhougou Formation of the Ming Tombs section places the age of the Changcheng Group at less than 1800 Ma (Wan et al., 2003). Our carbon isotope chemostratigraphy thus begins at ca. 1700 Ma in the late Paleoproterozoic.

The boundary age between the Jixian and Qingbaikou groups is ca. 1000 Ma based on a series of K–Ar ages for illites and glauconites from the Hongshuizhuang, Tieling, and Xiamaling formations (Lu et al., 1996). The ^{40}Ar–^{39}Ar ages for glauconite measured by Li et al. (1996) indicate that the ages of the Tieling and Jingeryu formations are ca. 1175–1070 Ma (±10 Ma) and ca. 900–810 Ma (±10 Ma), respectively, based on 1171 ± 11 Ma, 1125 ± 11 Ma and 1082 ± 13 Ma ages for the Tieling Formation and 880 ± 8.5 Ma, 842.2 ± 11.3 Ma, and 816.1 ± 8.9 Ma ages for the Jingeryu Formation. These estimates are consistent with a ca. 1000 Ma age for the contact between the Jixian and Qingbaikou groups and a ca. 800 Ma upper limit for the Qingbaikou Group (Lu et al., 1996). The contact ages between formations of the Jixian Group are also based on published data, including 1380 ± 24 Ma (chert Ar–Ar age) for the top of the Gaoyuzhuan Formation, 1317 ± 22 Ma (chert Ar–Ar age) for the top of Yangzhuang Formation, parallel 1206 ± 27 and 1208 ± 21 Ma (chert Ar–Ar ages) for the top of Wumishan Formation, and 1425 ± 21 Ma for the lower Gaoyuzhuang Formation (Wang et al., 1995). Galena Pb–Pb model ages of 1485 Ma, 1434 Ma, and 1384 Ma from a SEDEX Pb–Zn mine suggest an age of 1434 ± 50 Ma for the middle

Gaoyuzhuang Formation (Chung, 1977). A similar geochronological framework was adopted by (Li et al., 2003a,b) among others.

3. SAMPLE PREPARATION AND ANALYTICAL TECHNIQUES

A number of workers have used trace sulfate extracted from biotic and abiotic carbonates (CAS) to constrain the sulfur isotope composition of seawater when both Precambrian and Phanerozoic sequences lacked evaporite deposits (Ueda et al., 1990; Bottomley et al., 1992; Strauss, 1993; Hurtgen et al., 2002; Kah et al., 2004; Kampschulte and Strauss, 2004; Lyons et al., 2004a; Gellatly and Lyons, 2005). Recently, a comparison between several hundred data from biogenic calcites and whole rock carbonate samples and contemporaneous evaporites demonstrated that CAS in Phanerozoic marine carbonates likely records the primary sulfur isotope composition of seawater (Kampschulte and Strauss, 2004). Much of the scatter in the two data sets, particularly that observed in the early–mid Paleozoic CAS results, is now known to reflect primary, systematic variability illuminated by data generated at high stratigraphic resolution (Gill et al., 2007). In the process, Kampshulte and Strauss also confirmed the reliability of the whole-rock CAS approach, thus further opening the door for C and S isotope analysis of Proterozoic seawater (e.g., Hurtgen et al., 2004; Kah et al., 2004; Gellatly and Lyons, 2005). In the absence of skeletal carbonate, Precambrian CAS studies are dependent entirely on analysis of whole-rock micrite and dolomicrite, which dominate our sample set, including stromatolitic dolostone and limestone. The work of Kah et al. (2004) revealed good agreement between interbedded dolostone and gypsum, suggesting that very early-formed dolomites, with their comparatively low solubilities during diagenesis, might be particularly reliable archives of primary seawater chemistry.

3.1. Extraction of trace sulfate from carbonate

Sulfate is an important trace constituent of many marine carbonates, with abundances ranging from a few tens of ppm in inorganic precipitates to several thousand ppm in biogenic carbonates (Busenberg and Plummer, 1985). We used a common method involving sulfate precipitated as $BaSO_4$ to prepare CAS for sulfur isotope analysis (Burdett et al., 1989; Hurtgen et al., 2002; Gellatly and Lyons, 2005). For each sample, approximately 200 g of whole rock was crushed and then pulverized into powder of <200 mesh size using a carbide mill. Contaminated portions, such as weathered material or veins, were removed prior to powdering. About 50–100 g of carbonate powder was soaked in a 5.25% sodium hypochlorite (NaOCl) solution over 24 h and then rinsed with distilled water. The bleach step aids in the removal of water-soluble sulfates, including those deriving from pyrite oxidation. The bleach also enhances oxidation of labile sulfides and organic compounds. More generally, the removal of sulfate minerals, primary and secondary, is optimized by the addition of NaCl to the initial water rinse. However, we viewed this addition as an unnecessary step here because of the very low pyrite contents in most of our samples. The pretreated carbonates were then dissolved in 200 ml HCl (6 N) for 12 h at room temperature; the residue was removed by filtration and washed with distilled water. The pH value of the filtrate was adjusted to ~4 and heated to boil. Approximately 20 ml of saturated $BaCl_2$ solution was added to the boiling sample digest. The samples were heated for an additional 30 min and then allowed to cool. The $BaSO_4$ precipitate was filtered after 12 h. CAS concentrations were determined gravimetrically, with errors estimated to be within ±20%. The large error reflects the relatively small amount of precipitate.

3.2. Sulfur isotopic analysis

When 10 mg or more of $BaSO_4$ was available, SO_2 was generated through off-line combustion with V_2O_5 and SiO_2 at 1000 °C (Yanagisawa and Sakai, 1983). Sulfur isotope measurements were performed on a Finnigan Delta S mass spectrometer. Other samples with less than 10 mg of extracted $BaSO_4$ were combusted and analyzed by on-line elemental analyzer-mass spectrometry (EA-MS) as described by Glesemann et al. (1994).

Sulfur isotope ratios are expressed as per mil (‰) deviations from the S isotope composition of the Vienna Canon Diablo Troilite (VCDT) using the conventional $\delta^{34}S$ notation. Analytical uncertainties for sulfur isotope compositions are better than ±0.3‰ for the off-line method and ±0.5‰ for EA-MS. Working standards—GBW04414, GBW04415 (National Standard of China), and LTB-2—were measured for S isotope ratios using both methods. The $\delta^{34}S$ values relative to VCDT were −0.07‰ for GBW04414 (Ag_2S), +22.15‰ for GBW04415 (Ag_2S), and +1.84‰ for LTB-2 (pyrite).

3.3. C and O isotopic analyses

Dolomite was predominant in the analyzed samples, with minor limestone. We used a conventional off-line 100% H_3PO_4 method to produce CO_2 gas for mass spectrometric analysis (McCrea, 1950). Chemical reaction was carried out for 24 h at constant 25 °C for limestone and 50 °C for dolomite. Carbon and oxygen isotope analyses of the CO_2 were performed using a Finnigan Delta S mass spectrometer, and isotope compositions are expressed as $\delta^{13}C$ and $\delta^{18}O$ relative to VPDB. Analytical uncertainties for C and O isotope compositions are all better than ±0.2‰ (1σ).

3.4. Trace element analyses

We measured Ca, Mg, Mn, and Sr contents to evaluate post-depositional alteration of the carbonates. Because of the presence of chert in some intervals, samples were dissolved in a HF/HNO_3 solution and measured by inductively coupled plasma-optical emission spectrometry (ICP-OES). The reproducibility is better than ±10%, and detection limits are 0.05%, 0.05%, 10 mg/g, and 5 mg/g for Ca, Mg, Mn, and Sr, respectively.

4. RESULTS AND DISCUSSION

4.1. Evaluation of diagenetic alteration

A number of theoretical, experimental, and analytical studies of carbonate diagenesis show that trace element and isotope compositions of sedimentary carbonate rocks can change due to interaction with diagenetic and post-diagenetic fluids (Hudson, 1977; Brand and Veizer, 1980; Banner and Hanson, 1990; Banner, 1995; Kaufman and Knoll, 1995; Xiao et al., 1997; Jacobsen and Kaufman, 1999; Bartley et al., 2001). The water–rock ratio and differences between the primary compositions of the rock/sediment (and thus seawater) and the diagenetic fluids are the primary factors in determining the rates and extents of elemental and isotopic exchange in carbonate rocks. It is difficult to collect absolutely unaltered carbonate rocks in ancient sequences, particularly from the Precambrian, but screening techniques are available.

Carbon isotope data for the least altered carbonate samples are selected based on values for Mn/Sr and $\delta^{18}O$ (Knoll et al., 1995; Kaufman and Knoll, 1995; Xiao et al., 1997). Under the influence of diagenetic and/or post-diagenetic fluids, especially meteoric waters, Sr can be expelled from sedimentary carbonates, whereas Mn is often incorporated (Brand and Veizer, 1980), and oxygen isotope exchange with cycling meteoric waters can result in significant decreases in the $\delta^{18}O$ value of sedimentary carbonates (Kaufman and Knoll, 1995). Therefore, the degree of alteration can be estimated by using the Mn/Sr ratio and $\delta^{18}O$ value. Carbonates (limestones and dolostones) with Mn/Sr < 10 and/or $\delta^{18}O > -10‰$ are commonly considered to preserve primary $\delta^{13}C$ values (Kaufman and Knoll, 1995; Xiao et al., 1997). Diagenetic and post-diagenetic alteration, in principle, may also overprint the $\delta^{34}S$ value of CAS, because the sulfate primarily displaces the carbonate ion and is bound structurally in the carbonate mineral lattice (Takano, 1985). However, CAS may have an even stronger potential for preservation of primary seawater signals due to the much lower SO_4^{2-} contents of most diagenetic and/or post-diagenetic fluids relative to seawater. Recent work has shown that meteoric diagenesis can result in significant reductions in CAS concentration. Importantly, however, $\delta^{34}S_{CAS}$ is buffered to the primary seawater value even during conversion of aragonite to calcite under meteoric conditions (Lyons et al., 2005), and sediments showing high extents of early diagenetic sulfate reduction and corresponding shifts in the $\delta^{34}S$ of pore water sulfate can preserve primary seawater $\delta^{34}S$ (Lyons et al., 2004b). Bacterial sulfate reduction (BSR) can cause large isotope differences between seawater and pore water, yet the seawater CAS signal can remain intact even when carbonate cements are precipitating in the presence of the evolved sulfate pool, suggesting signal domination by the primary sediment (Lyons et al., 2004b). The integrity of the proxy is enhanced by the low residual sulfate concentrations within pore waters that have experienced extensive BSR. To be safe, however, we avoided lithologies with abundant organic matter, which is a controlling factor in determining rates of BSR.

Crossplots of $\delta^{13}C$ versus $\delta^{18}O$ and $\delta^{13}C$ versus Mn/Sr for carbonate units in the Changcheng and Jixian groups do not follow diagenetic trends (Fig. 4a–d), even though some samples in both groups have Mn/Sr ratios of more than 10, and some have $\delta^{18}O$ values of less than $-10‰$. In their evaluation of post-depositional alteration, Li et al. (2003b) suggested that the Ming Tombs and Jixian sections experienced two pathways of diagenesis that probably reset the primary carbon isotope composition of the carbonate rocks—silicification and diagenesis of organic matter. In the Jixian section, the dolomitic cherts and cherty dolostones from the Dahongyu, Gaoyuzhuang, and Wumishan formations commonly have Mn/Sr ratios much greater than 10 and/or $\delta^{18}O$ values less than $-10‰$ (Fig. 4a–d and Table 1), identical to the patterns in Ming Tombs section described by Li et al. (2003b). Post-depositional alteration may have significantly changed the $\delta^{13}C$ value of those samples but likely did not modify their $\delta^{34}S_{CAS}$ value (Lyons et al., 2004b, 2005).

For some of the samples with high Mn/Sr ratios, volcanism should be considered a factor in diagenesis. For example, the dolostones near the volcanic unit of the Tieling Formations (samples J7 to J24) contain extremely high Mn concentrations of ca. 1300–8800 ppm, which result in much higher Mn/Sr ratios (Fig. 4d). The hydrothermal activity associated with volcanism during the Tieling stage probably altered Mn and other chemical contents of primary carbonates, including those in the upper Hongshuizhuang Formation.

While the $\delta^{13}C$–$\delta^{18}O$ crossplot does show good correlation for the Jingeryu Formation of the Qingbaikou Group (Fig. 4e and also Fig. 2D of Li et al., 2003b), most of the samples of the Jingeryu have Mn/Sr ratios lower than 10 and $\delta^{18}O$ values higher than $-10‰$. Consistent with previous arguments (Xiao et al., 1997; Li et al., 2003b), we propose that most samples of the Jingeryu Formation have preserved primary geochemical signals , except for a few samples with Mn/Sr ratios of >10 or $\delta^{18}O$ values of $<-10‰$.

Sulfur, carbon, and oxygen isotope data of the Jixian section are summarized in Fig. 5. The rectangles, diamonds, and circles denote $\delta^{34}S_{CAS}$, $\delta^{13}C_{carbonate}$, and $\delta^{18}O_{carbonate}$ values, respectively. The open symbols indicate samples that fail to satisfy the criteria of $\delta^{18}O > -10‰$ and/or Mn/Sr < 10 and therefore suggest that the sample could have suffered a certain degree of diagenetic alteration. The least altered samples (with solid symbols) satisfy both these conditions and may therefore record the sulfur and carbon isotope compositions of contemporaneous seawater (i.e., dissolved sulfate and carbonate in ocean) (e.g., Strauss, 1993; Kaufman and Knoll, 1995; Strauss, 1997).

It is clear that altered samples have (1) larger $\delta^{13}C_{carbonate}$ variation than the unaltered or least altered samples and (2) relatively depleted $\delta^{13}C_{carbonate}$ values. In contrast, differences in $\delta^{34}S_{CAS}$ between the unaltered and altered samples are comparatively minor. This relationship and above discussion indicate that diagenetic and post-diagenetic alteration can affect $\delta^{13}C_{carbonate}$ with negligible impact on the sulfur isotope composition of the CAS, as suggested by Lyons et al. (2004b);Lyons et al. (2005). Further,

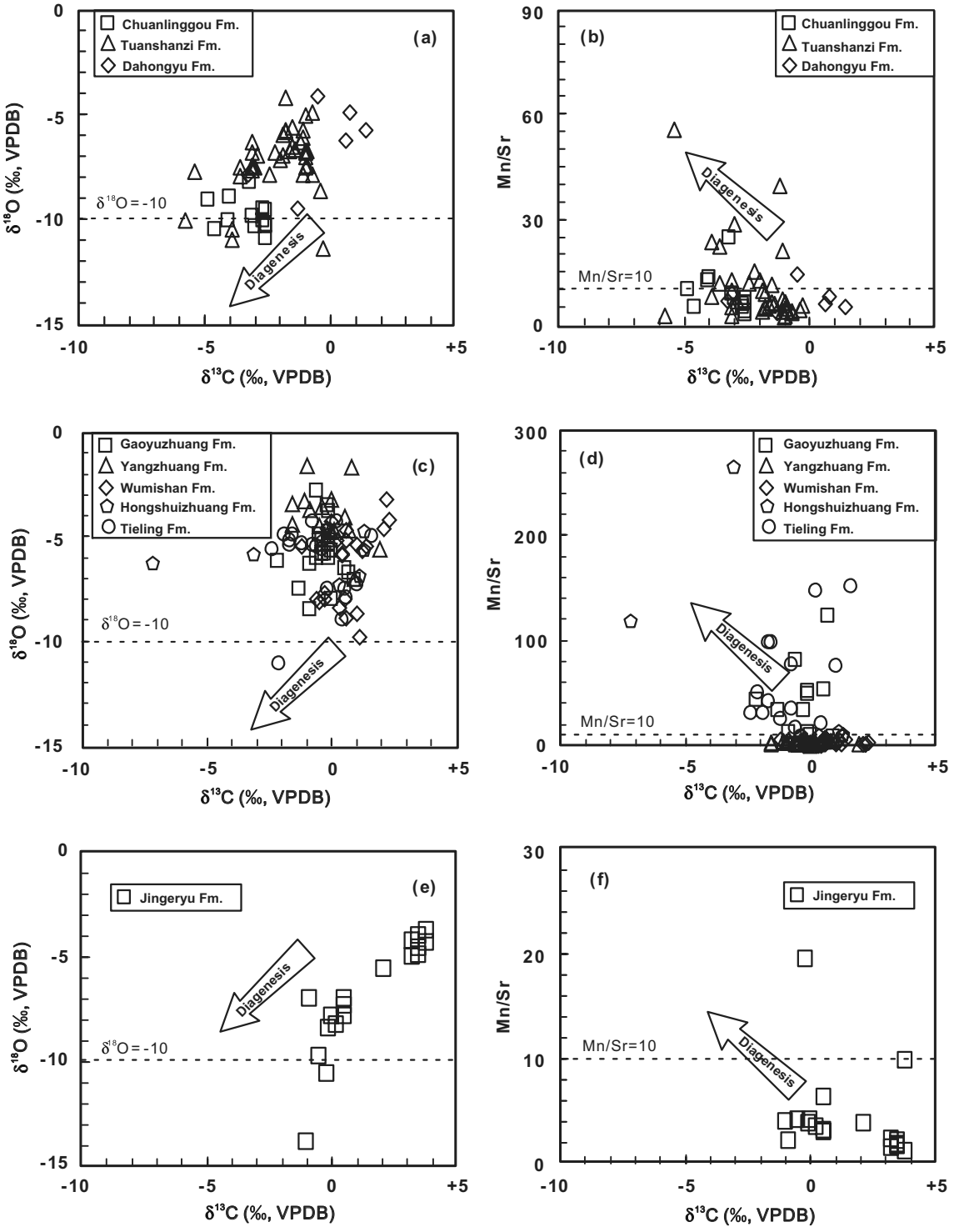

Fig. 4. Crossplots of $\delta^{18}O$ and Mn/Sr versus $\delta^{13}C$: (a) $\delta^{18}O$–$\delta^{13}C$ for the Changcheng Group, (b) Mn/Sr–$\delta^{13}C$ for the Changcheng Group, (c) $\delta^{18}O$–$\delta^{13}C$ for the Jixian Group, (d) Mn/Sr–$\delta^{13}C$ for the Jixian Group, (e) $\delta^{18}O$–$\delta^{13}C$ for the Qingbaikou Group, and (f) Mn/Sr–$\delta^{13}C$ for the Qingbaikou Group.

primary carbon isotope compositions often remain unchanged in sedimentary carbonates during diagenetic and post-diagenetic alteration of the sediments and rock. Commonly, the carbonate–carbon reservoir is also large relative to the carbon in diagenetic fluids. Consequently, $\delta^{13}C$ values are less sensitive to diagenetic overprinting than $\delta^{18}O$ and Mn/Sr (Hudson, 1977). The curves for the $\delta^{34}S$ (including the $\delta^{34}S$ data of the altered samples) and $\delta^{13}C$ (excluding the $\delta^{13}C$ data of the clearly altered samples) of the Jixian marine carbonates in Fig. 6 can reflect secular

Table 1
Elemental and isotopic compositions of Proterozoic carbonates in the Jixian section, northern China

Sample	Lithology[a]	Height[b] (m)	$\delta^{34}S$ (‰), VCDT	$CaSO_4$ (ppm)	$\delta^{13}C$ (‰), VPDB	$\delta^{18}O$ (‰), VPDB	CaO (%)	MgO (%)	Mn (ppm)	Sr (ppm)	Mn/Sr (wt)
Chuanlinggou Fm.		0									
J106	arg./Dol.	732.5	32.9	537	−4.0	−9.0	29.41	8.93	1856	139	13.35
J107	arg./Dol.	734	34.5	267	−2.6	−10.9	15.36	5.87	758	200	3.79
J108	arg./Dol.	736			−4.1	−10.1	29.23	7.66	1231	98	12.56
J109	arg./Dol.	738	26.0	560	−4.9	−9.1	27.52	7.98	1006	100	10.06
J110	Dol.	741	34.4	199	−2.7	−10.1	14.43	6.88	777	131	5.93
J111	Dol.	748.4			−2.6	−10.3	9.97	4.64	492	157	3.13
J112	arg./Dol.	752.4			−2.6	−10.4	26.47	6.97	693	91	7.62
J113	Dol.	757.3	30.3	179	−2.6	−9.6	23.53	8.9	921	148	6.22
J114	Dol.	761.3	31.6	406	−2.7	−9.5	14.54	7.54	709	137	5.18
J115	Dol.	764.4			−3.0	−10.4	13.73	7.43	898	122	7.36
J116	Dol.	766.2			−3.1	−9.9	14.65	7.56	954	108	8.83
J118	Dol.	775.9	28.3	698	−3.2	−8.3	20.22	10.32	1784	72	24.78
J119	Dol.	778		46	−4.6	−10.5	6.26	4.29	797	155	5.14
Tuangshanzi Fm.		889									
J120	Dol.	889.1			−3.9	−11.0	3.5	2.86	1098	47	23.36
J121	Dol.	897.5	24.4	179	−5.4	−7.8	13.71	12.29	2103	38	55.34
J122	Dol.	907.9			−3.0	−7.6	17.92	10.33	1693	59	28.69
J123	Dol.	916.5		62	−2.2	−6.9	21.09	11.16	1812	119	15.23
J124	Dol.	927.2			−3.6	−7.6	17.18	9.01	1988	168	11.83
J125	Dol.	941.5	26.0	90	−3.1	−7.7	12.17	7.63	934	182	5.13
J126	Dol.	947.3			−3.1	−7.5	0.17	1.02	67	28	2.39
J127	Dol.	950.5			−2.9	−7.0	15.62	8.46	1105	165	6.7
J128	Dol.	963.3			−3.1	−6.9	14.4	8.73	1184	125	9.47
J129	Dol.	973.3			−3.1	−6.4	17.13	9.94	1239	97	12.77
J130	Dol.	993.3	31.3	440	−3.9	−10.5	13.06	8.27	918	113	8.12
J131	Dol.	999.1			−2.4	−7.9	12.5	8.03	972	84	11.57
J132	Dol.	1003.8			−2.0	−7.2	10.22	6.53	1281	102	12.56
J133	Dol.	1015.8			−1.9	−7.0	0.22	0.35	257	26	9.88
J134	Dol.	1025.3			−1.2	−6.4	16.05	9.3	1982	50	39.64
J135	Dol.	1032.3		99	−1.1	−6.2	10.59	6.72	1312	63	20.83
J136	Dol.	1054.4			−1.5	−5.7	16.51	9.07	1140	178	6.4
J137	Dol.	1065.4			−3.6	−8.0	22.15	11.01	1923	86	22.36
J138	Dol.	1073.5	30.2	168	−1.5	−6.6	22.68	12.35	1052	93	11.31
J139	Dol.	1085.4			−1.0	−7.1	11.75	7.17	610	94	6.49
J140	Dol.	1096.2			−0.3	−11.4	4.85	3.49	269	48	5.6
J141	Dol.	1106.2	29.1	152	−1.6	−6.8	14.7	8.88	656	116	5.66
J142	Dol.	1115.9			−5.8	−10.1	6.29	7.32	1218	471	2.59
J143	Dol.	1130.6			−1.1	−7.9	4.59	3.08	401	55	7.29
J144	Dol.	1182.6			−0.7	−7.9	3.45	2.35	261	81	3.22

J145	Dol.	1212.3			−1.0	−7.6	0.74	0.34	113	43	2.63
J146	Dol.	1232.3		354	−0.9	−7.5	3.58	2.62	219	58	3.78
J147	Dol.	1248			−1.4	−6.7	9.68	6.61	390	67	5.82
J149	Dol.	1265			−0.9	−6.8	13.89	8.83	530	116	4.57
J150	Dol.	1279			−1.0	−6.8	0.22	0.15	111	63	1.76
J151	Dol.	1287.3	5.8	575	−1.0	−5.1	14.25	9.69	619	140	4.42
J152	Dol.	1308			−0.4	−8.7	2.7	1.94	269	65	4.14
J153	Dol.	1318			−1.0	−6.9	1.94	1.62	331	51	6.49
J154	Dol.	1327.3			−1.8	−4.3	11.85	8.11	711	158	4.5
J155	Dol.	1331	25.9	141	−1.1	−5.8	10.04	6.6	574	157	3.66
J156	Dol.	1339.2	27.2[c]	350	−0.7	−5.0	18.16	10.38	1081	281	3.85
J157	Dol.	1349	12.8	216	−1.9	−6.0	2.45	1.38	227	57	3.98
J159	Dol.	1390			−1.8	−5.9	0.04	0.05	226	25	9.04
J158	Dol.	1407			−1.8	−5.8	0.09	0.13	285	57	5
Dahongyu Fm.		1417									
J161	Dol.	1457			1.4	−5.8	19.42	11.96	881	173	5.09
J162	chert/Dol.	1460			−1.3	−9.5	5.94	3.7	239	69	3.46
J163	chert/Dol.	1463			0.6	−6.3	3.88	2.26	470	78	6.03
J165	Dol.	1587			0.8	−5.0	23.09	13.13	1041	132	7.89
J166	chert/Dol.	1604			−3.3	−7.9	9.79	0.98	277	40	6.93
J168C	Dol.	1803			−0.5	−4.2	12.71	8.68	423	30	14.1
Gaoyuzhuang Fm.		1815.1									
J169	chert/Dol.	1815.2	16.4	178	0.0	−8.0	0.26	0.18	226	24	9.42
J170	Dol.	1816			−0.3	−5.8	16.13	10.52	1401	42	33.36
J173	chert/Dol.	1817.5			0.9	−7.1	7.91	4.94	743	84	8.85
J176	chert/Dol.	1819.7	16.0	241	−0.9	−8.5	2	1.39	230	19	12.11
J181	chert/Dol.	1827.7			−1.3	−7.5	9.79	5.82	1206	36	33.5
J182	Dol.	1850.6	24.6	187	−0.1	−5.2	26.77	14.16	2185	42	52.02
J184	Dol.	1872.4			0.5	−6.5	19.15	11.72	898	17	52.82
J186	Dol.	1913.7	24.4	218	−0.1	−6.0	23.33	13.28	1600	33	48.48
J194	Dol.	2026.1	29.0	558	0.7	−6.7	22.23	12.57	2458	20	122.9
J198	Dol.	2089.9	27.6	479	−2.2	−6.2	17.12	10.88	1677	38	44.13
J204	Dol.	2179.6			−0.6	−2.8	26.25	15.02	1801	22	81.86
J218	Lms.	2399.3			−0.9	−6.3	48.51	0.97	116	118	0.98
J228	Dol.	2563.6			−0.1	−3.8	14	9.54	374	29	12.9
J236	Lms.	2704.9			−0.1	−5.3	50.13	3.29	62	478	0.13
J242	dol./Lms.	2815.5			−0.6	−6.0	35.8	8.88	83	308	0.27
J253	Dol.	3007.3	17.1[c]	89	−0.2	−3.5	33.12	11.01	69	209	0.33
J267	Dol.	3260.2			0.0	−5.7	29.45	15.89	24	16	1.5
J269	Dol.	3290.6			−0.1	−4.8	29.7	16.25	20	13	1.54
J271	Dol.	3301.7			−0.4	−5.8	30.38	16.34	21	17	1.24
J273	Dol.	3306.4			−0.4	−5.1	26.11	15	19	22	0.86
J280	Dol.	3316.9			−0.5	−4.9	29.01	15.21	32	28	1.14
Yangzhuang Fm.		3317									
J287	Dol.	3320.6			−0.2	−4.9	29.28	16.24	108	26	4.15
J289	Dol.	3339.4		75	−0.5	−4.5	24.28	14.13	62	35	1.77

(*continued on next page*)

Table 1 (*continued*)

Sample	Lithology[a]	Height[b] (m)	$\delta^{34}S$ (‰), VCDT	$CaSO_4$ (ppm)	$\delta^{13}C$ (‰), VPDB	$\delta^{18}O$ (‰), VPDB	CaO (%)	MgO (%)	Mn (ppm)	Sr (ppm)	Mn/Sr (wt)
J292	Dol.	3375	10.8	123	−1.6	−3.4	21.16	11.92	100	42	2.38
J293	Dol.	3389.3	12.9	344	−0.4	−3.6	27.85	15.19	80	61	1.31
J295	Dol.	3436.7	17.6	179	0.0	−4.8	29.78	15.93	44	50	0.88
J296	Dol.	3452.4	23.2	212	−1.1	−3.3	20.45	12.87	146	38	3.84
J305	Dol.	3523.7	15.9	164	−1.6	−4.4	24.84	14.51	48	38	1.26
J309	Dol.	3583.7	20.5	876	−0.9	−3.7	20.72	13.25	148	29	5.1
J319	Dol.	3714.2	17.9	486	−1.0	−1.6	23.43	14.23	159	48	3.31
J326	Dol.	3781.8	15.8[c]	88	0.1	−4.7	19.23	12.19	107	25	4.28
J330	Dol.	3830.5			1.9	−5.6	28.16	16.09	31	28	1.11
J340	Dol.	3971.7	20.8	314	0.0	−3.2	22.8	13.61	167	302	0.55
J381	Dol.	3982.8	19.8	193	0.7	−4.7	30.24	16.11	173	46	3.76
J384	Dol.	3994.4	15.0	240	0.8	−1.7	20.07	13.21	118	31	3.81
J386	Dol.	4001.3	24.6	350	0.5	−4.1	30.27	16.46	190	45	4.22
J391	Dol.	4010.7	23.4	278	0.9	−7.0	20.31	12.94	151	28	5.39
Wumishan Fm.		4011									
J392	Dol.	4011.3	23.3	291	−0.5	−8.1	28.13	15.84	148	178	0.83
J396	Dol.	4017.4			1.0	−8.7	29.09	16.01	67	31	2.16
J397	Dol.	4022.6	22.9	259	−0.3	−7.7	28.35	15.74	162	31	5.23
J401	Dol.	4339.3			0.4	−5.8	29.13	16.15	19	19	1
J413	Dol.	4800.7			−0.2	−4.6	29.89	16.24	37	39	0.95
J418	Dol.	5056.4			1.0	−5.4	29.64	16.09	27	24	1.13
J423	Dol.	5206.9			0.0	−4.3	29.48	15.43	67	25	2.68
J427	Dol.	5310.2	18.5[c]	72	0.2	−5.2	27.91	15.47	49	39	1.26
J430	Dol.	5375			−1.2	−5.5	30.19	16.52	120	24	5
J437	Dol.	5605.2			−0.6	−8.0	28.74	16.06	45	34	1.32
J438	Dol.	5634.7			0.6	−5.2	22.38	12.87	169	22	7.68
J442	Dol.	5795.7			0.6	−4.7	28.48	16.02	30	41	0.73
J447	Dol.	6214.3			0.5	−8.0	29.56	16.3	29	20	1.45
J451	Dol.	6359.6			0.4	−5.9	28.76	16.08	26	37	0.7
J457	Lms.	6649.6			−0.3	−8.0	53.23	0.4	10	79	0.13
J459	Dol.	6805.5			0.3	−8.4	24.35	13.38	10	25	0.4
J464	Dol.	7161.3			1.2	−5.7	29.97	16.59	35	21	1.67
J465	Dol.	7228.7	19.8	194	2.1	−4.6	28.54	14.66	82	43	1.91
J476	Dol.	7282.5	24.8	268	2.3	−4.2	29.76	16.38	70	33	2.12
J475	Dol.	7297.5			2.2	−3.2	24.45	14.43	76	42	1.81
J472	Dol.	7323.3			0.6	−8.9	29.84	16.2	131	18	7.28
J471	Dol.	7331.9			1.1	−9.8	30.48	15.54	130	23	5.65
J466	Dol.	7346.7			1.4	−5.5	28.61	14.46	154	27	5.7
Hongshuizhuang Fm.		7347									
J341	arg./Dol.	7347.7			1.3	−4.7	24.91	13.39	230	29	7.93
J342	arg./Dol.	7351.1	29.6[c]	117	1.3	−5.6	21.41	12.87	281	26	10.81

J343	arg./Dol.	7353.5			0.3	−7.3	22.26	13.09	238	24	9.92
J344	arg./Dol.	7357.4			1.1	−6.9	23.71	12.99	303	23	13.17
J345	arg./Dol.	7359.4	23.4	246	−0.4	−5.2	4.95	3.85	155	16	9.69
J351	arg./Lms.	7410.1		63	−7.2	−6.3	35.18	1.5	8909	76	117.22
J352	arg./Dol.	7414.3	20.0	155			23.91	11.05	6367	56	113.7
J357	arg./Dol.	7439.2	15.1	120			0.42	0.38	1047	6	174.5
J359	arg./Dol.	7441.4	10.3	717	−3.1	−5.8	6.81	0.84	2122	8	265.25
Tieling Fm.		7447.8									
J7	Dol.	7448.2			−2.1	−11.1	18.54	11.08	5129	103	49.8
J8	Dol.	7448.8	29.4	223	−1.7	−5.4	22.8	12.73	5533	56	98.8
J9	Dol.	7451.9	27.4	152	1.6	−5.0	23.94	12.73	8808	58	151.86
J10	Dol.	7458.7	29.2	180	−1.6	−4.9	20.01	12.23	5316	54	98.44
J11	Dol.	7460.9	31.5	228	−1.7	−5.2	25.81	13.95	2432	58	41.93
J12	Dol.	7464	33.8	185	−2.4	−5.6	25.29	13.53	1926	62	31.06
J14	Dol.	7476.1	32.3[c]	61	−1.9	−4.9	26.94	14.39	1347	43	31.33
J18	Dol.	7492.7			−0.8	−4.3	27.67	14.49	2453	32	76.66
J21	Dol.	7507.7			1.0	−7.3	27.53	14.5	2665	35	76.14
J24	Dol.	7527.7			0.2	−4.3	26.74	13.73	5745	39	147.31
J32	Lms.	7592.7			0.5	−7.5	39.36	0.82	124	47	2.64
J39	dol./Lms.	7657.7			0.6	−7.9	41.1	8.59	290	63	4.6
J43	dol./Lms.	7682.7	24.8	122	0.4	−9.0	32.21	12.95	822	38	21.63
J46	Lms.	7697.7			−0.2	−7.5	50.85	0.56	131	50	2.62
J53	Lms.	7757.7			−0.4	−5.6	46.92	1.67	1125	129	8.72
J54	Lms.	7767.7			−0.6	−5.5	49.63	0.99	1366	84	16.26
J55	Dol.	7778.7	32.4[c]	109	−1.2	−5.3	40.45	2.87	1845	74	24.93
J56	dol./Lms.	7778.7	33.9	216	−0.8	−5.4	41.08	4.41	2502	71	35.24
Xiamaling Fm.		7779									
J60	arg./Lms.	7858.9	25.4[c]	110							
J66	arg./Lms.	7945.2	33.2[c]	68							
Jingeryu Fm.		8064.7									
J105	Lms.	8064.7	24.6	225	3.8	−4.4	41.24	0.87	1811	184	9.84
J103	Lms.	8066.7	32.3	321	3.5	−4.7	44.67	0.61	390	213	1.83
J101	Lms.	8070.7			3.2	−4.3	46.62	0.58	352	234	1.5
J100	Lms.	8072.7	32.3	370	3.5	−5.0	45.29	0.67	364	229	1.59
J98	Lms.	8077.2			3.2	−5.1	46.89	0.68	370	160	2.31
J96	Lms.	8080.7	33.8	201	3.5	−4.1	46.14	0.76	435	207	2.1
J94	Lms.	8084.7	26.0[c]	175	3.8	−3.8	48.86	0.58	332	266	1.25
J90	Lms.	8092.7			−0.9	−7.1	31.01	0.83	270	126	2.14
J89	Lms.	8094.7			2.1	−5.7	42.82	0.61	377	100	3.77
J85	Lms.	8104.2	22.6[c]	50	0.5	−7.4	36.91	1.18	494	152	3.25
J80	Lms.	8116	18.3[c]	455	0.5	−7.1	37.44	0.59	513	170	3.02
J76	Lms.	8140.6			0.2	−8.3	18.03	2.06	603	172	3.51
J75	Lms.	8144.9	31.7	98	0.0	−7.9	24.74	1.73	629	151	4.17
J74	Lms.	8150.4			0.5	−7.9	14.8	2.51	571	91	6.27
J73	Lms.	8152.4			−0.1	−8.5	25.73	1.26	580	152	3.82

(*continued on next page*)

Table 1 (*continued*)

Sample	Lithology[a]	Height[b] (m)	$\delta^{34}S$ (‰), VCDT	$CaSO_4$ (ppm)	$\delta^{13}C$ (‰), VPDB	$\delta^{18}O$ (‰), VPDB	CaO (%)	MgO (%)	Mn (ppm)	Sr (ppm)	Mn/Sr (wt)
J72	Dol.	8159.2			−0.2	−10.7	13.11	8.61	274	14	19.57
J71	Dol.	8163.3	29.9	1412	−1.0	−13.9	21.99	11.48	185	46	4.02
J70	Dol.	8164			−0.5	−9.8	19.49	12.25	237	57	4.16
Fujunshan Fm.		8165									
J68	Lms.	8167	31.6	785	31.6	1.07	47.80	2.41	73	322	0.23

[a] Abbreviations: arg./Dol., argillaceous dolostone; dol., dolostone; chert/Dol., cherty dolostone; Lms., limestone; arg./Lms., argillaceous limestone; dol./Lms., dolomitic limestone.
[b] Measured thickness when sampling.
[c] Measured by using EA-MS.

isotopic variations in global seawater during that period of geological history.

4.2. Isotope chemostratigraphy

We present fewer sulfur isotope data than carbon and oxygen results, which are generally continuous in the Jixian section (Figs. 5 and 6). In some formations, particularly the Gaoyuzhuang and Wumishan, insufficient CAS was available for S isotope analysis. The concentration of seawater sulfate in the mid-Proterozoic may have been lower than that of the later Neoproterozoic and Phanerozoic due to the lower level of atmospheric oxygen (Canfield and Teske, 1996; Canfield, 1998; Shen et al., 2003; Kah et al., 2004; Lyons et al., 2004a, 2005; Gellatly and Lyons, 2005). Shen et al. (2003) estimated that mid-Proterozoic seawater sulfate concentrations were probably within the range of 0.5–2.4 mM, which is about 2–10% of the present concentration of 28 mM. Similarly, Kah et al. (2004) argued for sulfate concentrations of roughly 5–15% of the modern value. General scarcity of sulfate in many of our samples is consistent with a low sulfate mid-Proterozoic ocean. Also, meteoric diagenesis is known to reduce CAS concentrations (Lyons et al., 2005). Furthermore, a data gap of about 10^8 years exists between the Xiamaling and Changlongshan formations in the lower Qingbaikou Group because of the absence of carbonate deposits in both formations; two $\delta^{34}S_{CAS}$ data were obtained from the Xiamaling Formation through sulfate extraction from its calcareous shale.

4.2.1. Late Paleoproterozoic Changcheng Group

$\delta^{34}S_{CAS}$ values in the Changcheng Group are high from +26.0‰ to +34.5‰, but the $\delta^{13}C_{carbonate}$ data are mostly negative, ranging from −4.9‰ to −2.6‰ in the carbonaceous dolomite of Member III of the Chuanlinggou Formation. When the data with $\delta^{18}O \leqslant -10$‰ and $Mn/Sr \geqslant 10$ are excluded, $\delta^{34}S_{CAS}$ and $\delta^{13}C_{carbonate}$ values range from +30.3‰ to +31.6‰ and from −3.1‰ to −2.6‰, respectively. In the overlying Tuanshanzi Formation, $\delta^{34}S_{CAS}$ values vary from +5.8‰ to +31.3‰, and the $\delta^{13}C$ values of dolomite vary between −3.1‰ and −0.8‰ for the least altered samples. Carbon isotope compositions increase from less than −3.0‰ at the base of the unit to −0.8‰ and then decrease to −1.8‰ in the upper portions of the unit. A total of 56 $\delta^{13}C_{carbonate}$ values from the two formations are reported (Table 1 and Fig. 5).

Six carbonate carbon isotope results for the Dahongyu Formation of the upper Changcheng Group vary between −3.3‰ and +1.4‰. The values are close to 0‰ near the top of the Dahongyu Formation. Unfortunately, we were not able to generate $\delta^{34}S_{CAS}$ data for this formation due to intensive silicification.

For the same time period (ca. 1700–1600 Ma), comparable carbon isotope data were reported from the McArthur and Mount Isa basins, Australia (Brasier and Lindsay, 1998; Lindsay and Brasier, 2000; Lindsay and Brasier, 2004). Lindsay and Brasier (2000) concluded that $\delta^{13}C$ values from ca. 1700 to 1575 Ma carbonates vary within a very narrow range around a mean of −0.6‰, with extreme values seldom lying further than 1‰ from the mean. However,

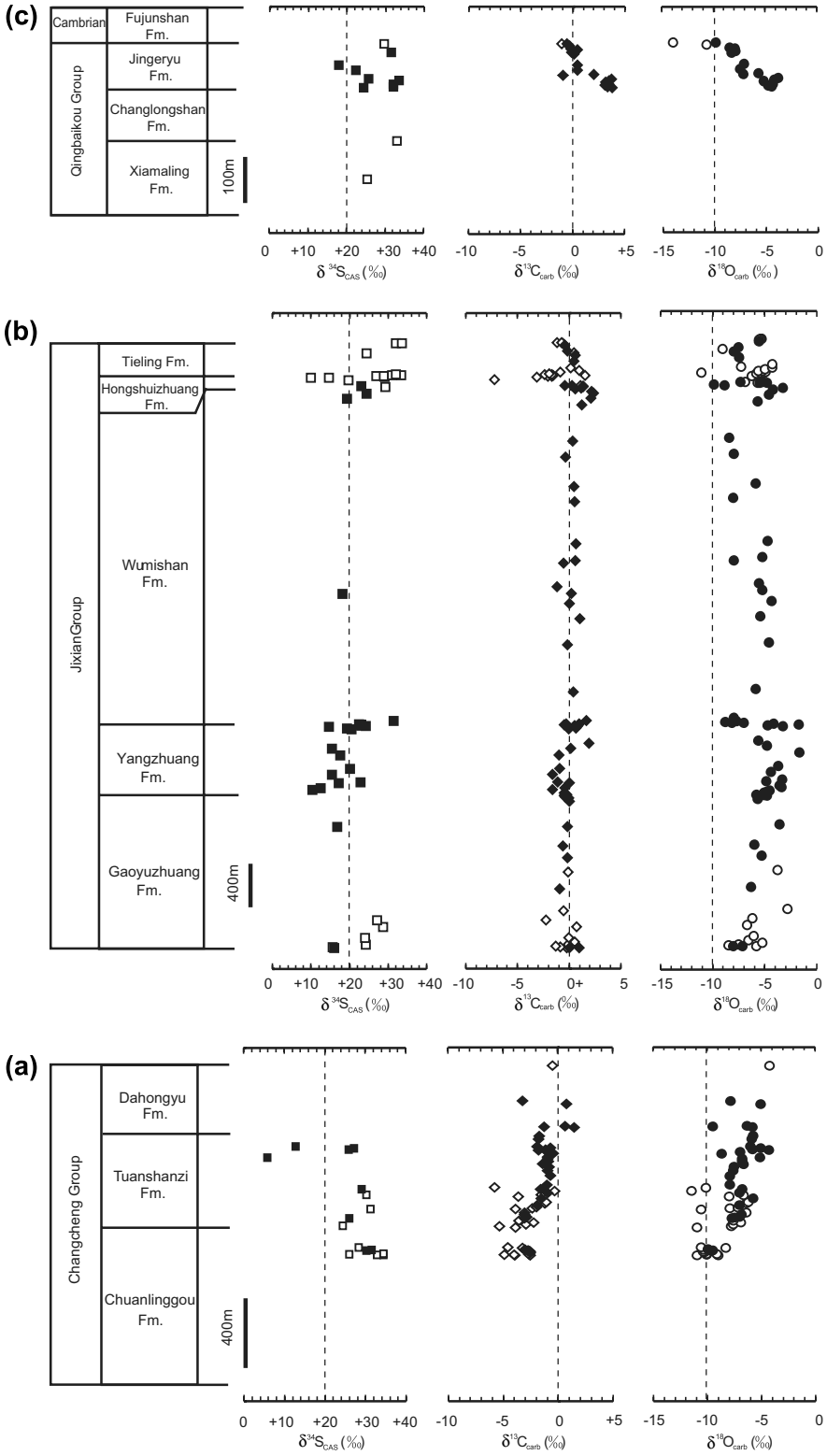

Fig. 5. Chemostratigraphy of $\delta^{34}S_{CAS}$, $\delta^{13}C_{carb}$, and $\delta^{18}O_{carb}$ for carbonates from the Jixian carbonate successions: (a) the Changcheng Group, (b) the Jixian Group, and (c) the Qingbaikou Group. Proterozoic stratigraphic successions and thickness are based on and Lu et al. (1996). Solid and open symbols denote the least altered and altered samples, respectively (see text for discussion).

a ~2‰ increase in $\delta^{13}C$ was observed at the ~1700 Ma base of the McArthur and McNamara groups (Lindsay and Brasier, 2000).

In the Changcheng Group from ca. 1700 to 1600 Ma, $\delta^{13}C_{carbonate}$ values are mostly negative and exhibit an ascending trend from approximately −3‰ to ~0‰. From

the base of Tuanshanzi Formation to the top of Gaoyuzhuang Formation, $\delta^{13}C$ values fluctuate considerably around 0‰. The observed ~3‰ increase in $\delta^{13}C$ is comparable to the ~2‰ decrease of Lindsay and Brasier (2000). The $\delta^{34}S_{CAS}$ values decrease up section, and the sulfur isotope data for the Chuanlinggou and Tuanshanzi formations closely match those from the ca. 1700 Ma Paradise Creek Formation of the McNamara Group, Australia (Lyons et al., 2004a; Kah et al., 2004; Gellatly and Lyons, 2005), and both $\delta^{34}S_{CAS}$ data sets suggest that the $\delta^{34}S$ of seawater for the late Paleoproterozoic may have exceeded 30‰ (Fig. 7a and b).

4.2.2. Mesoproterozoic Jixian Group

$\delta^{13}C_{carbonate}$ values for the Gaoyuzhuang dolomites in the Jixian Group fall mainly in a range of -0.5 ± 0.5‰, with a few results higher than 0‰ or lower than −1‰. The carbon isotope data are very stable over the 1500 m of the Gaoyuzhuang Formation. Such invariance is consistent with previous data from the Jixian section (Xiao et al., 1997) and the adjacent Ming Tombs section (Zhong and Chen, 1992; Li et al., 2003b). The $\delta^{34}S_{CAS}$ values reveal a positive excursion, rising to +29.0‰ in the lower part of the formation and then a decrease, dropping to +17.1‰.

Relative to the Gaoyuzhuang Formation, $\delta^{13}C_{carbonate}$ values from the Yangzhuang Formation show larger fluctuations within the range of −1.6‰ to +1.9‰, and $\delta^{34}S_{CAS}$ values fluctuate significantly in a range between approximately +10‰ and +25‰. $\delta^{34}S_{CAS}$ and $\delta^{13}C_{carbonate}$ variations are not completely synchronous within the Yangzhuang carbonate succession (Fig. 6). The Yangzhuang Formation (ca. 1400 Ma) shows $\delta^{34}S_{CAS}$ values similar to those of the Newland and Helena formations of the ca. 1450 Ma Belt Supergroup, Montana, U.S.A., reported by Lyons et al. (2004a), Kah et al. (2004), and Gellatly and Lyons (2005) (Fig. 7c–e).

The thick Wumishan section yielded only limited $\delta^{34}S_{CAS}$ data, and most of the analyses are concentrated near the top and bottom of the formation. As such, the sulfur isotope curve remains poorly defined for this formation, with $\delta^{34}S_{CAS}$ values that vary around +20‰ (Figs. 5 and 6). $\delta^{13}C_{carbonate}$ values fall mostly in a range of $+0.8 \pm 1.5$‰, which is comparable to the previous Wumishan data from the Jixian and Ming Tombs sections (Zhao, 1995; Zhao et al., 1997; Xiao et al., 1997; Li et al., 1999, 2003b).

Most samples from the Hongshuizhuang and Tieling formations can be classified as altered based on their

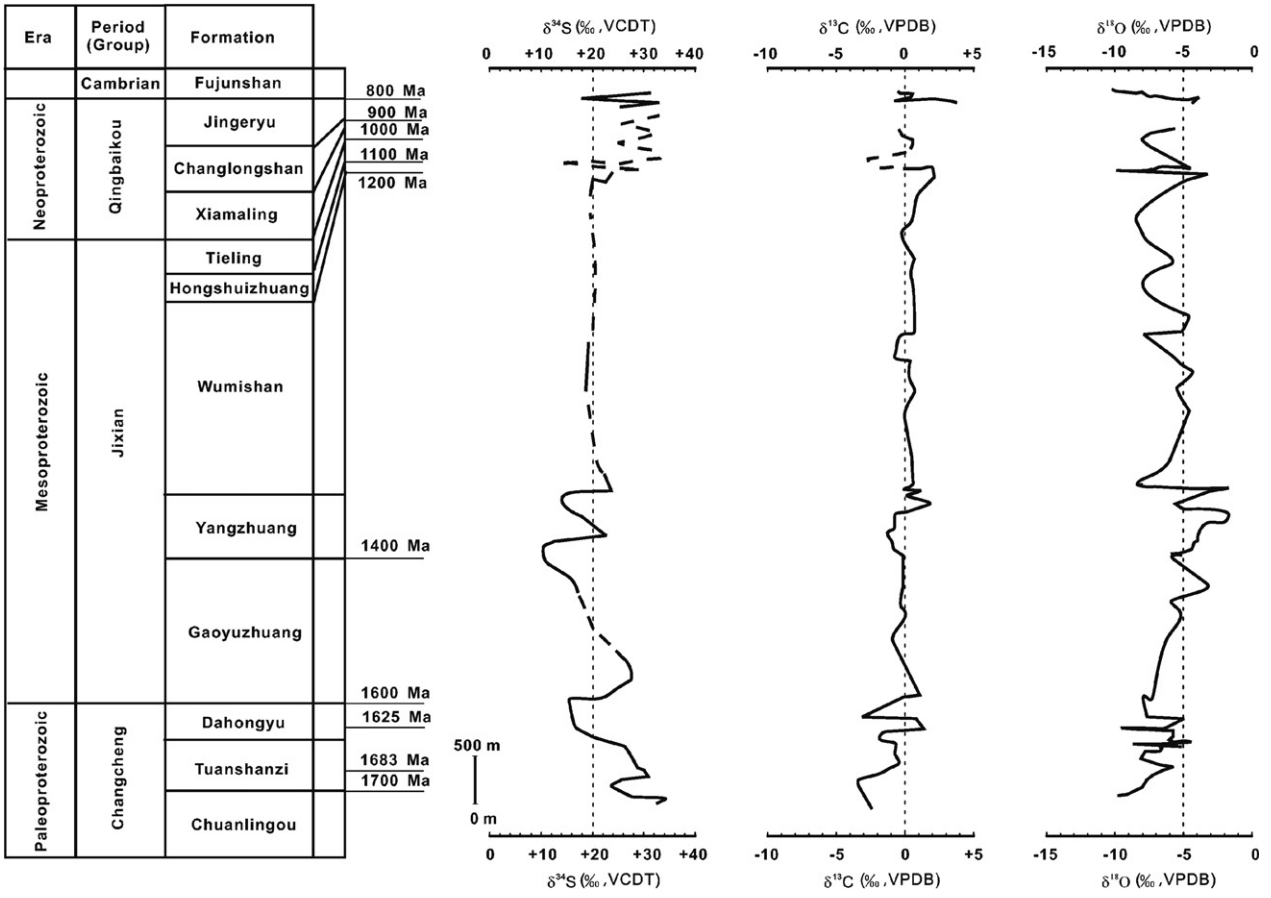

Fig. 6. Estimated evolution of $\delta^{34}S$ for CAS and $\delta^{13}C$ and $\delta^{18}O$ for carbonates from the Jixian carbonate successions. See text for stratigraphic ages. Dashed lines delineate uncertain intervals due to a lack of data. The trends for $\delta^{13}C$ and $\delta^{18}O$ are based primarily on the unaltered or least altered samples, but the $\delta^{34}S$ line for CAS includes altered samples because there is no significant difference between the altered and least altered materials.

$\delta^{18}O$ and Mn/Sr properties. In the Hongshuizhuang Formation, $\delta^{34}S_{CAS}$ values decrease up section from +29.6‰ to +10.3‰ in concert with $\delta^{13}C_{carbonate}$ values that decrease from +1.3‰ to −3.1‰. The range of $\delta^{34}S_{CAS}$ values for the Hongshuizhuang Formation is broad but still comparable to data from the 1200 Ma Mescal Limestone of the Apache Group, U.S.A., reported by Lyons et al. (2004a), Kah et al. (2004), and Gellatly and Lyons (2005) (Fig. 7f and g). In the stromatolitic limestone of the upper member of the Tieling Formation, $\delta^{13}C$ values are stable at ~0 ± 1‰. $\delta^{13}C_{carbonate}$ values, which are relatively low in the Jixian Group, vary between −2.4‰ and −1.6‰ in the lower member of the Tieling Formation. In contrast, the $\delta^{34}S_{CAS}$ values are relatively high, with the average exceeding +30‰. Approaching the top of the Tieling Formation, $\delta^{34}S_{CAS}$ values vary from approximately +25‰ to +33‰, with $\delta^{13}C_{carbonate}$ values that range from roughly +1‰ to −1‰. Similar $\delta^{13}C$ trends in the Tieling Formation were reported by Wang and Chen (1993).

4.2.3. Early Neoproterozoic Qingbaikou Group

Limestone is only present in the upper part of the Qingbaikou Group, specifically within the Jingeryu Formation of the Jixian section. Positive $\delta^{13}C_{carbonate}$ values close to +4‰ characterize the bottom of the formation and decrease progressively to ~−0.5‰ at the top of the unit, which is consistent with the data of Li et al. (2000). $\delta^{34}S_{CAS}$ increases from +24.6‰ at the bottom of section to ~+33‰ in the upper part and then decreases gradually to +18.3‰ in the Jingeryu Formation. Only near the Jingeryu and Fujunshan boundary does $\delta^{34}S_{CAS}$ return to higher values of ~+30‰. We obtained only two $\delta^{34}S_{CAS}$ values, +25.4‰ and +33.2‰, in the Xiamaling Formation of the Qingbaikou Group; these are similar to data from the upper Tieling Formation. Low carbonate contents prevented us from extracting trace sulfate from additional samples. There is a ca. 10^8 year hiatus in the $\delta^{13}C_{carbonate}$ record, so it is not clear how the data trend between the ~−0.5‰ value at the top of the Tieling Formation to ~+4‰ at the bottom of the Jingeryu Formation.

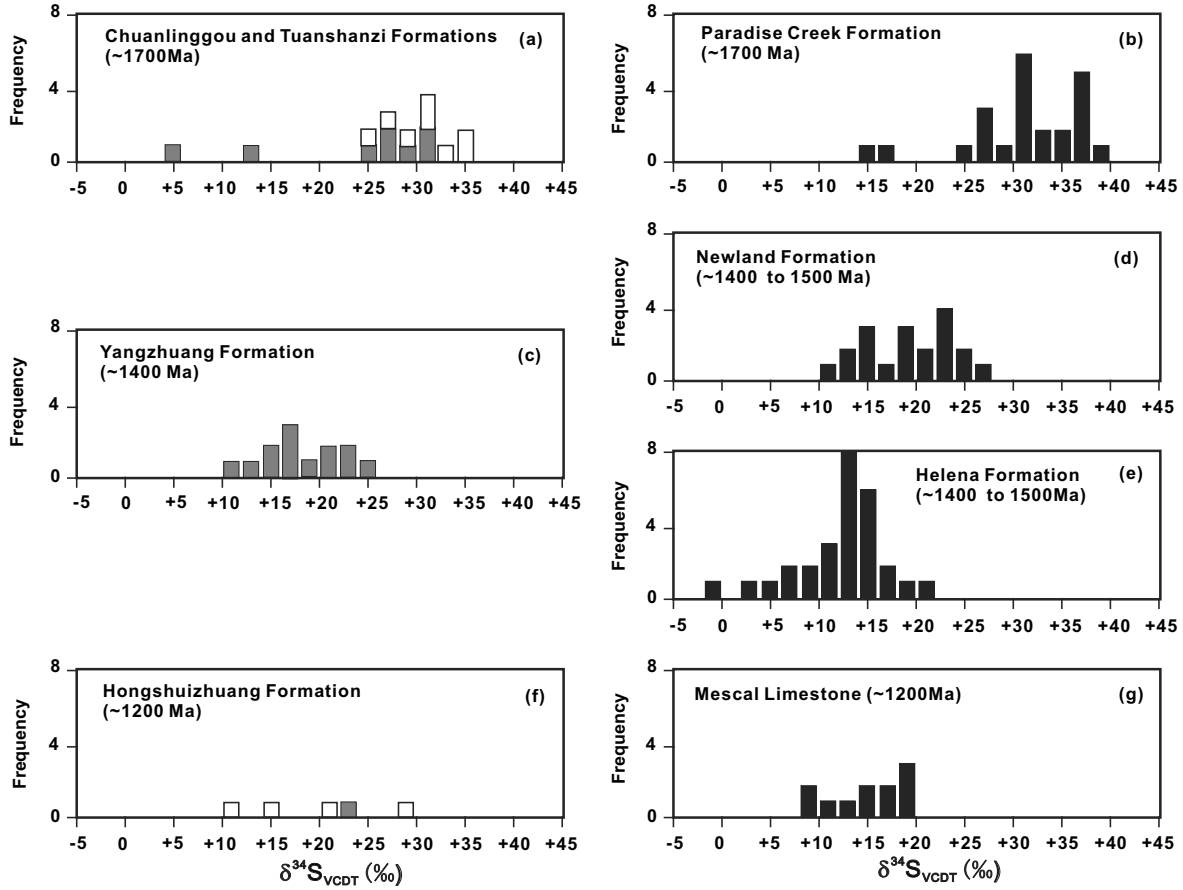

Fig. 7. Sulfur isotope data for carbonate-associated sulfate (CAS): (a) Chuanlinggou and Tuanshanzi formations, Changcheng Group, northern China; (b) Paradise Creek Formation, McNamara Group, Queensland, Australia (~1700 Ma); (c) Yangzhuang Formation, Jixian Group, northern China (~1400 Ma); (d) Newland Formation, Belt Supergroup, Montana, USA (~1400–1500 Ma); (e) Helena Formation, Belt Supergroup, Montana, USA (~1400–1500 Ma); (f) Hongshuizhuang Formation, Jixian Group, northern Chen et al. (1980)China (~1200 Ma); (g) Mescal Limestone, Apache Group, Arizona, USA (~1200 Ma); and (h) Society Cliffs Formation, Arctic, Canada (~1200 Ma). Open symbols denote altered samples. The data in figures (b), (d), (e), (g), and (h) are from Kah et al. (2001, 2004) and Gellatly and Lyons (2005).

4.3. S and C isotope records of Proterozoic marine sulfates and carbonates

Chemical marine sediments—sulfates and carbonates—that precipitate in isotopic equilibrium with past ocean waters have been used to trace the sulfur and carbon isotope evolution of ancient seawater. For example, secular variations in C and S isotope compositions are valuable stratigraphic tools and biogeochemical indicators for the late Neoproterozoic (ca. 850–543 Ma), permitting relatively fine-scale global correlation (Kaufman and Knoll, 1995; Brasier et al., 1996; Kaufman et al., 1997; Gorjan et al., 2000; Walter et al., 2000; Strauss, 2002; Shields et al., 2004). Pronounced fluctuations in the C and S isotope composition observed during this interval most likely record similarly strong changes in climate, global C and S biogeochemical cycling, and the atmospheric oxygen budget (Derry et al., 1992; Knoll, 1992; Des Marais, 1994; Canfield and Teske, 1996; Strauss, 1997; Hoffman et al., 1998; Hurtgen et al., 2002; Strauss, 2002). In contrast to the late Neoproterozoic, earlier Proterozoic C and S isotope variations are not well constrained.

The geological record contains abundant carbonates, but occurrences of sulfate evaporite deposits are limited in Precambrian strata (Strauss, 1993). Sulfur isotope data for Precambrian marine sulfate minerals (principally gypsum and anhydrite) have been presented in relatively few publications as reviewed by Claypool et al. (1980), Holser et al. (1988) Schidlowski (1989), Bottomley et al. (1992), and Strauss (1993, 2002). More recently, data for the S isotope evolution of Proterozoic marine sulfate spanning ca. 1800–800 Ma (Fig. 8) are available in Strauss (1993, 2002), Shields and Veizer (2002), Kah et al. (2001, 2004), Gellatly and Lyons (2005), and this study, among others. This later work relies heavily on CAS as a seawater proxy.

In addition to the above-mentioned McNamara Group (Fig. 7b), data from the McArthur Group, Australia, in which major sulfate evaporite deposits have been reported (Walter and Veevers, 1997), are comparable to the Changcheng Group. The age of the Barney Creek Formation in the McArthur Group lies between 1638 ± 7 and 1642 ± 6 Ma (Page and Sweet, 1998). $\delta^{34}S$ values for barite with gypsum pseudomorphs from the McArthur Group range from +19‰ to +32‰, with an average of +26.3‰ (Walker et al., 1983; Strauss, 1993), while the $\delta^{34}S$ values for sulfides are mostly positive with a minimum value at −7.4‰ and a maximum of +33.1‰ (Strauss, 2002). Recently, Kah et al. (2004) and Gellatly and Lyons (2005) reported many data for $\delta^{34}S_{CAS}$ from the McNamara Group that exceed +30‰ to +35‰ (Fig. 7b). Similarly high $\delta^{34}S_{CAS}$ values were obtained from the lower Chuanlinggou Formation, extending to the Tuanshanzi Formation in the Jixian carbonate succession. Similarities among data from the Changcheng, McNamara, and McArthur groups imply that the $\delta^{34}S$ of seawater attained values exceeding +30‰ during the late Paleoproterozoic at ca. 1600–1700 Ma. However, $\delta^{34}S$ values lower than +15‰ have also been observed in this interval (Figs. 7a, b and 8). Short-term variability in the sulfur cycle can be driven by reoxidation of bacterially derived H_2S and pyrite during oceanic mixing and by rapid pyrite burial under widespread euxinic conditions (Canfield, 1998; Newton et al., 2004; Bottrell and Newton, 2006). The superposition of short-term variability (e.g., this study, Kah et al., 2004; Gellatly and Lyons, 2005) on the first order curve results in the complexity seen in Fig. 7. Such variability is consistent with generally low sulfate concentrations in the Proterozoic ocean.

The later Mesoproterozoic (ca. 1300–1100 Ma) and the earlier Neoproterozoic (ca. 1000–800 Ma) are two other time intervals for which high $\delta^{34}S$ values are observed (Fig. 8). For the lower Tieling Formation at ca. 1100 Ma, $\delta^{34}S_{CAS}$ values of +30‰ are considered to reflect contemporaneous seawater, even though the carbonates experienced possible hydrothermal metasomatism as indicated by the exceptionally high Mn concentrations. Consistent with this interpretation, the high $\delta^{34}S$ values for evaporites and CAS from the Society Cliffs Formation, Canada (Kah et al., 2001; Strauss, 2002; Kah et al., 2004; Lyons et al., 2004a) (Fig. 7h), and the Grenville Series, USA (Strauss, 1993), are similar to the $\delta^{34}S_{CAS}$ values of the Tieling Formation. Estimates for the ages of marine $CaSO_4$ evaporites are ca. 1200 Ma for the Society Cliffs Formation (Kah et al., 2001; and references therein) and ca. 1100 Ma for the Grenville Series (Strauss, 1993). From top of the Tieling Formation to the lower Jingeryu Formation (Table 1), most $\delta^{34}S_{CAS}$ values exceed +30‰. These results imply that Neoproterozoic seawater at ca. 1000–800 Ma had high $\delta^{34}S$ values (Fig. 8).

Relatively low $\delta^{34}S$ values, a maximum of ~25‰, occurred during the Yangzhuang stage at ca. 1400 Ma (Fig. 8). Similar $\delta^{34}S$ values have been reported for CAS from the Newland Formation of the Belt Supergroup (Lyons et al., 2004a; Gellatly and Lyons, 2005) at ca. 1450 Ma. Both $\delta^{34}S$ data sets vary by ~15‰ (Fig. 7c and d).

In contrast to the $\delta^{34}S$ values, $\delta^{13}C_{carbonate}$ data from the Jixian section are relatively stable and vary within a range of around 0 ± 5‰ when only the least altered samples are considered (Fig. 9). Based on this $\delta^{13}C$ behavior, the interval between ca. 1700 and 800 Ma can be considered isotopically "quiet" relative to the two glacial periods of the early Paleoproterozoic and late Neoproterozoic (Fig. 1). However, marine carbonate samples from the Jixian section still suggest appreciable variation in the $\delta^{13}C$ of Proterozoic seawater, generally corresponding to the trends observed for $\delta^{34}S$. For example, from the late Paleoproterozoic to the early Mesoproterozoic, $\delta^{34}S_{CAS}$ decreased from ~+34‰ to ~+16‰, while $\delta^{13}C$ values increased from ~−3‰ to ~0‰. During the Mesoproterozoic at ca. 1400 Ma, $\delta^{34}S$ values fluctuated over a 10‰ range, with >3‰ variation in $\delta^{13}C$ within ~700 m thickness of the Yangzhuang Formation. In addition, $\delta^{13}C_{carbonate}$ increases of >2‰ and decreases of >4‰ are observed in two intervals—ca. 1300–1200 Ma and ca. 900–800 Ma, respectively. These excursions correspond with the two periods of high $\delta^{34}S_{CAS}$ exceeding +30‰ (Figs. 5, 6, 8 and 9). These new data challenge previous assertions of C and S isotope stability throughout the Mesoproterozoic (also Frank et al., 1997, 2003; Bartley and Kah, 2004).

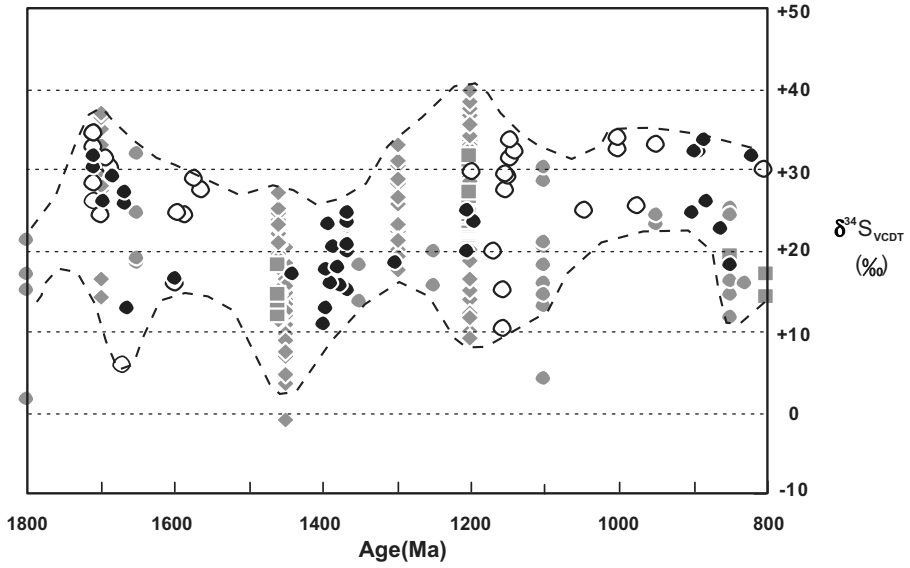

Fig. 8. Estimated sulfur isotope variation in late Paleoproterozoic to early Neoproterozoic seawater. Background sulfate data plotted as gray symbols: circles are from the PMCID 1.1a database of Shields and Veizer (2002); squares are from Strauss (1993), Kah et al. (2004), and Gellatly and Lyons (2005). Solid and open black circles denote the least altered and altered samples, respectively, from the Jixian section, and the age for the each sample is obtained by interpolation based on the stratigraphical thickness and ages listed in Fig. 6. The two dashed lines define the possible range of seawater $\delta^{34}S$ values from 1800 Ma to 800 Ma.

Unlike the Phanerozoic (Berner, 2001), and despite some general correspondence in the $\delta^{34}S_{CAS}$ and $\delta^{13}C_{carbonate}$ records, sulfur isotope perturbations in the global sulfate reservoir appear to be decoupled from carbon isotope variation in marine carbonates during the Proterozoic Era (Fig. 10). Such isotopic decoupling, however, does not preclude coupled C–S redox cycling during the Proterozoic. Based on model results suggesting that the Mesoproterozoic sulfate reservoir was only about 5–15% the size of the modern ocean reservoir, Kah et al. (2004), Lyons et al. (2004a), and Gellatly and Lyons (2005) inferred that relatively rapid variations in $\delta^{34}S_{sulfate}$ were likely driven by the short-term relationships among weathering inputs, ocean ridge-related hydrothermal activity, and the extent of sulfate reduction and associated pyrite burial—all of which had enhanced isotopic expressions under the lower concentrations (and thus shorter residence time) of sulfate. Conversely, high dissolved inorganic carbon (DIC) contents in the Proterozoic ocean, as evidenced by inferred high levels of calcium carbon saturation, likely suppressed the isotopic variability in the oceanic carbon reservoir. In the Neoproterozoic to earliest Paleozoic, the size of the marine sulfate reservoir increased as related to increased ocean-atmosphere oxygenation, including the deep ocean, along with a decrease in the DIC content linked to metazoan skeletization—although sulfate concentrations remained well below those that typified younger strata (Canfield, 2004; Gill et al., 2007). The balance of these processes, as modulated through feedback processes, led to the coupling of the C and S isotope systems that generally characterizes the Phanerozoic (e.g., Kurtz et al., 2003; Bartley and Kah, 2004; Canfield, 2004; Fike et al., 2006).

4.4. Implication for global events

Earlier published data indicate that Mesoproterozoic seawater sulfate possessed relatively low, uniform $\delta^{34}S$ values around +15‰ to +20‰ (Bottomley et al., 1992; Strauss, 1993), and carbonate $\delta^{13}C$ values fell in a narrow range of about +1‰ to +2‰ (Buick et al., 1995; Knoll et al., 1995). The isotopic stability suggested by Buick et al. (1995) based on published C and S data might be attributed to severe nutrient limitations on primary productivity. Such limitations could have been a driving force creating photosymbiotic associations in eukaryotic cells (Brasier and Lindsay, 1998). Despite these earlier interpretations, however, the growing geological and biogeochemical evidence suggests that the Mesoproterozoic may have been a time of significant change in the global carbon and sulfur cycles, the biogeochemical cycles of redox sensitive elements, and evolutionary diversification in both prokaryotic and eukaryotic communities (Kah and Bartley, 2001). In fact, multicellular algae were discovered in the lowermost Changzhougou Formation of Paleoproterozoic Changcheng Group (ca. 1800 Ma) (Zhu et al., 2000). Global tectonic events—specifically the breakup of Columbia, a pre-Rodinia supercontinent, and subsequent assembly of the Rodinia supercontinent (Condie, 1998; Yale and Carpenter, 1998; Rogers and Santosh, 2002; Zhao et al., 2002, 2004)—could be linked to those major biogeochemical transitions and thus would have influenced the cycles for carbon and sulfur (Kah and Bartley, 2001; Luepke and Lyons, 2001; Lindsay and Brasier, 2002). Global tectonic events can imprint the $\delta^{13}C$ and $\delta^{34}S$ records in sedimentary rocks, particularly shifts in $\delta^{34}S_{sulfate}$ at times of reduced sulfate concentrations (Kah et al., 2004; Lyons et al., 2004a). Global tectonic events that may have driven

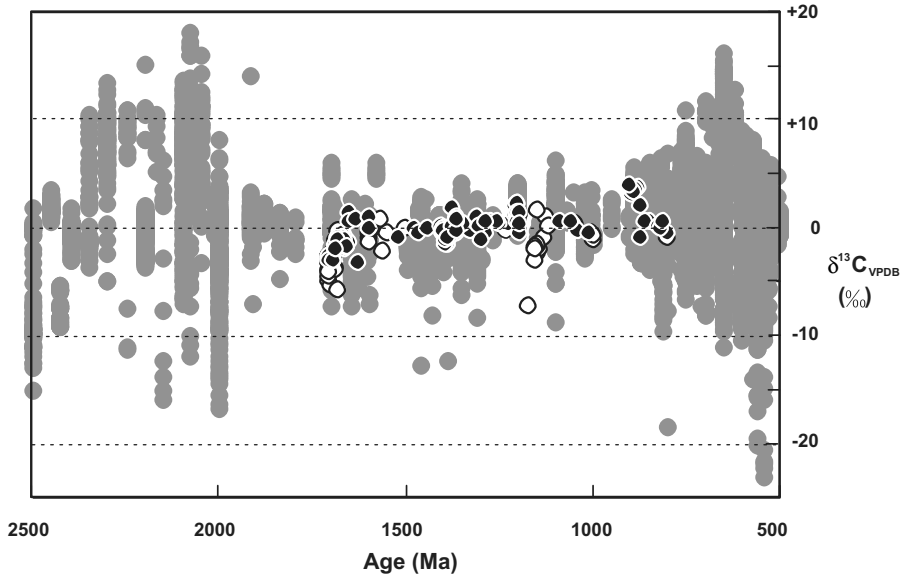

Fig. 9. $\delta^{13}C$ data for Proterozoic marine carbonates plotted against time. The background $\delta^{13}C$ range is shown as gray circles, which are plotted based on PMCID 1.1a database of Shields and Veizer (2002). Solid and open black circles denote the least altered and altered samples, respectively, from the Jixian section, and the age for the each sample is obtained by calculation from the stratigraphical thickness and ages listed in Fig. 6.

carbon and sulfur isotope variations in Proterozoic seawater are shown here (Fig. 11).

In the fourth subformation of Wumishan Formation in Jixian section, a >2‰ rise in $\delta^{13}C$ (Figs. 5 and 6) might correlate with ~3–4‰ positive shifts in ca. 1250–1300 Ma carbonate successions from Siberia, Russia, and the Dismal Lakes Group, Canada (Bartley et al., 2001; Frank et al., 2003; Bartley and Kah, 2004). Beginning in the late Mesoproterozoic at some time between 1300 and 1200 Ma, the carbon isotope record gradually became more variable, with a trend that oscillated from around −1‰ to as much as +4‰ (Knoll et al., 1995). Variability gradually increased until by 800 Ma, in the late Neoproterozoic, when the curve achieved exceptionally high values of up to +11‰—similar to those seen during the glacial episodes in the early Paleoproterozoic (Fig. 1). In addition to their relationships to Neoproterozoic glaciation, these isotopic developments appear to occur in parallel with the assembly and early breakup of Rodinia (Lindsay and Brasier, 2004).

Frequently rapid shifts in $\delta^{34}S_{sulfate}$ of more than 10‰ occurred at ca. 1300–1100 Ma (Fig. 8). The large excursions within the interval from the top of the Wumishan Formation to lower part of the Tieling Formation in the Jixian section, China, and in the Society Cliffs Formation and the Dismal Lakes Group, Canada (Kah et al., 2001, 2004), are examples of this variability. These isotopic shifts seem to be associated generally with stepwise assembly of Rodinia (Fig. 11e). Equally rapid isotopic variation is unknown from late Paleozoic and younger successions but is recorded in sulfate data from several Proterozoic successions, suggesting that the oceanic sulfate reservoir was small and much more sensitive to the flux imbalance that drove rapid sulfur isotope variations during the Proterozoic and early Paleozoic (Kah et al., 2004; Gill et al., 2007). During periods of supercontinental assembly, intracontinental seaways are well developed, bacterial sulfate reduction intensifies, and oceanic sulfate concentration decreases due to an increased input of nutrients to the oceans and thus greater organic carbon production. Secular variations in the sulfur isotope composition of seawater sulfate are typically attributed to changes in the burial ratio of reduced versus oxidized forms of sulfur. Positive excursions in $\delta^{34}S$ represent the preferential removal of ^{32}S from the oceans via an increase in the fraction of total sulfur buried as pyrite (Berner and Raiswell, 1983). A period of mountain building can also result in increased pyrite and organic carbon burial due to high siliciclastic accumulation rates, causing an in-phase rise in the $\delta^{34}S$ and $\delta^{13}C$ of contemporaneous seawater analogous to that beginning with the fourth subformation of the Wumishan Formation.

During a period of rifting, shown in Fig. 11b, high rates of organic carbon burial along an increasing length of continental margin can result in a significant rise in the $\delta^{13}C_{carbonate}$ value, such as that spanning the Chuanlinggou and Tuanshanzi formations of the Changcheng Group. A rise in the $\delta^{13}C$ of carbonates is clearly recorded in stratigraphic units spanning the late Paleoproterozoic to Paleo-Mesoproterozoic boundary (ca. 1700–1600 Ma) (Figs. 5, 6 and 9). Des Marais (2001) suggested that carbon isotope compositions were relatively stable in marine carbonates from ca. 1800 to 1000 Ma. However, a significant rise is also seen in the data of Xiao et al. (1997) and Li et al. (2003b). The collision of two old continental blocks resulted in final assembly of the Columbia supercontinent at ca. 1850 Ma (Fig. 11a), which formed the crystalline basement of the North China Craton (Zhao et al., 2002, 2004), followed by strong mountain building in the central zone (Guo et al., 2001; Zhao et al., 2003). The eastern part of

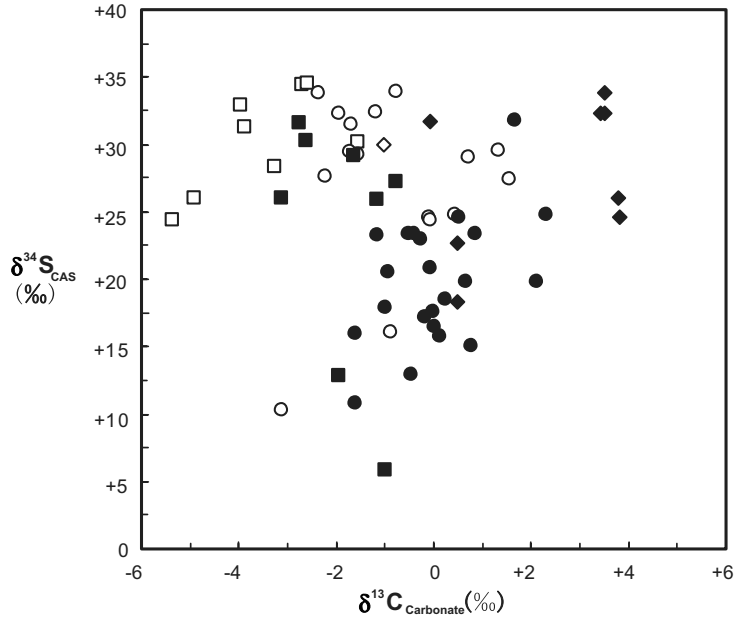

Fig. 10. Crossplot of $\delta^{34}S$ versus $\delta^{13}C$. Squares, circles, and diamonds represent Changcheng, Jixian, and Qingbaikou groups, respectively, and open and solid symbols denote the altered and least altered samples, respectively.

North China Craton experienced a tectonic transformation from compression to extension, reflecting a global rifting stage (Fig. 11b), and an intracontinental basin centered in Jixian region began to form around 1750 Ma. Potassium-rich volcanic rocks in the Tuanshanzi and Dahongyu formations indicate that dramatic extension persisted in this region to the end of the Paleoproterozoic (Fig 11b and c). The North China Craton, comparative to the contemporaneous Svecofennide and North American cratons, was considered to experience the same global event of continental breakup (Zhai et al., 2000). This event corresponds with the onset of breakup of the Columbia supercontinent (Zhao et al., 2002, 2004), as shown in Fig. 11b. In the Jixian section, the persistent rise and subsequent fluctuation in dolomite $\delta^{13}C$ that spans the Chuanlinggou and Dahongyu formations may be a response to the breakup of Columbia. A $\delta^{13}C$ excursion and fluctuations similar to those of the Jixian section have been reported from the ca. 1700–1500 Ma carbonate successions in the Mount Isa and McArthur basins, Australia (Brasier and Lindsay, 1998).

The global-scale breakup of Columbia in the Mesoproterozoic (Zhao et al., 2002, 2004) should also be reflected in the sulfur isotope compositions of contemporaneous seawater. In fact, the evaporites from the McArthur Group, Australia, and CAS from the McNamara Group, Australia, and the Changcheng Group, China, all record high $\delta^{34}S$ values of over +30‰ (Figs. 7a, b and 8, and the references associated with these figures). The ^{34}S enrichments imply enhanced rates of bacterial sulfate reduction and burial of biogenic pyrite during the global continental breakup (i.e., development of rift basins) starting at ca. 1800 Ma, even though atmospheric oxygen levels during the Paleo- and Mesoproterozoic were significantly lower than those of the late Neoproterozoic, and sulfur isotope fractionation between sulfate and biogenic sulfide may only have been about 25–30‰ (Canfield and Teske, 1996; Canfield, 1998; Johnston et al., 2005; Fike et al., 2006). However, the $\delta^{34}S$ of seawater would decrease gradually as intracontinental basins opened and juvenile oceanic crust formed; associated hydrothermal activity and alteration of ocean crust would release considerable amounts of mantle-derived sulfur into the oceans.

The global oceans and continents entered a relatively equable period during the Mesoproterozoic. This period is depicted in Fig. 11c. Fluctuations in $\delta^{34}S$ and $\delta^{13}C$ at ca. 1450–1400 Ma (Figs. 7c–e, 8 and 9), recorded in the carbonate successions of the Yangzhuang Formation, China, and the Belt Supergroup, U.S.A. (Frank et al., 2003; Lyons et al., 2004a; Kah et al., 2004; Gellatly and Lyons, 2005), may be related to large-scale magmatic activity at the end of breakup of the Columbia supercontinent (Zhao et al., 2002, 2004), as shown in Fig. 11d. During the period of supercontinental transition, subduction was initiated, and island-arcs and back-arc basins were produced. Subduction of biogenic carbon reservoirs into the mantle and lower crust preferentially removed lighter carbon from the biosphere, leaving the global ocean enriched in heavy carbon and the atmosphere richer in oxygen, which would promote a positive shift in $\delta^{13}C_{carbonate}$ (Lindsay and Brasier, 2002). Similarly, a positive shift in $\delta^{34}S$ for sulfate could happen through enhanced removal of biogenic pyrite enriched in ^{32}S from the oceanic reservoir because of possible widespread euxinic and suboxic conditions in the Proterozoic (Canfield, 1998, 2004; Arnold et al., 2004). Also, in island-arc settings, episodic volcanic activity would expel large amounts of gas derived from subducted materials and degassing of mantle. Through these processes, considerable amounts of isotopically light sulfur and carbon,

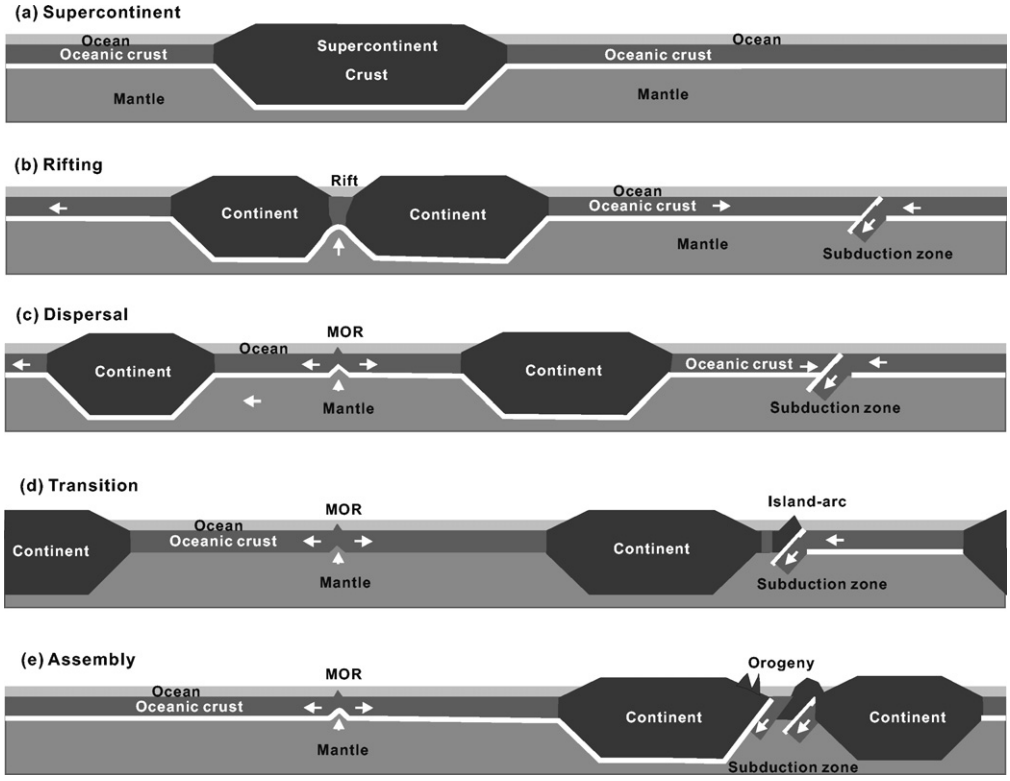

Fig. 11. Hypothetical tectonic evolution recorded in the geochemical data: (a) supercontinent formation, (b) onset of rifting during supercontinent (Columbia) breakup, (c) continent dispersal following supercontinent breakup, (d) transition from breakup to supercontinent (Rodinia) assembly, and (e) stepwise continental collision and amalgamation.

mostly the previously buried and subducted pyrite and organic carbon, would be reintroduced to the global atmosphere-oceanic system. These factors probably caused fluctuations in $\delta^{34}S$ and $\delta^{13}C$ during periods of tectonic transition.

5. SUMMARY AND CONCLUSIONS

The Proterozoic carbonate-dominated Jixian succession appears to record secular variations in $\delta^{34}S$ and $\delta^{13}C$ of seawater from ca. 1700 Ma to ca. 800 Ma. $\delta^{13}C$ values are mostly negative in the range of 0‰ to −3‰ for the late Paleoproterozoic at ca. 1700–1600 Ma and remain stable at $\sim 0 \pm 1$‰ through most of the Mesoproterozoic. Positive values of $+2 \pm 2$‰ characterize the early Neoproterozoic at ca. 900–800 Ma. In contrast to the $\delta^{13}C$ data, secular variations in $\delta^{34}S$ of seawater are dramatic, with high values exceeding +30‰ in the early Neoproterozoic. $\delta^{34}S$ values are mostly greater than +25‰, and only a few are less than +15‰ in the late Paleoproterozoic. In the early Mesoproterozoic, the $\delta^{34}S$ values are relatively low and vary mostly within a range of about +5‰ to +25‰. However, the $\delta^{34}S$ returns to high values of more than +30‰ with large fluctuations in the late Mesoproterozoic.

During the late Paleoproterozoic from ca. 1700 to 1600 Ma, the remarkable 10‰ decrease in $\delta^{34}S$ and ~3‰ increase in $\delta^{13}C$ for seawater are likely related to the breakup of the Columbia supercontinent. At the beginning of supercontinent breakup, enhanced rates of organic carbon and pyrite burial, which would reflect high extents of bacterial sulfate reduction in the sediments and possibly the Proterozoic water column and increased siliciclastic iron delivery, may have resulted in higher $\delta^{34}S$ and $\delta^{13}C$ values for Paleoproterozoic seawater. High accumulation rates would also increase the burial efficiencies of organic carbon and pyrite, and ^{34}S enrichments would be exacerbated by lower concentrations of sulfate in the Proterozoic ocean; however, with alteration of juvenile oceanic crust during the extension of intracontinental basins, seawater may have returned to the previous low $\delta^{34}S$ values through inputs of mantle-derived sulfur.

For the $\delta^{34}S$ and $\delta^{13}C$ of seawater, significant fluctuations at ca. 1450–1400 Ma, in contrast to earlier claims of Mesoproterozoic isotopic stability, may reflect the end of Columbia breakup. During this stage, subduction and large-scale magmatic activity were initiated in island-arc areas. Organic carbon and pyrite would be removed from oceans and enter the mantle and lower crust by subduction and thus would result in increases in both the $\delta^{34}S$ and $\delta^{13}C$ of contemporaneous seawater. At the same time, a considerable amount of sulfur and carbon delivered to the lower crust and mantle would be expelled by episodic volcanic activity. As a result, the $\delta^{34}S$ and $\delta^{13}C$ values of seawater at ca. 1450–1400 Ma fluctuated dramatically.

From the late Mesoproterozoic (ca. 1300–1100 Ma) to the early Neoproterozoic (ca. 800 Ma), representing the assembly and early breakup of Rodinia, global seawater is characterized by high values and large fluctuations of

$\delta^{34}S$ and $\delta^{13}C$ at ca. 1300–1100 Ma and 1000–900 Ma. Several factors, such as increasing weathering and nutrient input, enhanced primary productivity and bacterial sulfate reduction, and high siliciclastic burial rates, promoted increases in $\delta^{34}S$ and $\delta^{13}C$ values during this period. Clearly, changes in paleoceanographic conditions linked to global tectonic reorganization influenced C and S biogeochemical cycles, driving variation in the C and S isotope compositions of contemporaneous seawater on a variety of timescales. As we are now seeing in complementary studies of the early Paleozoic, we expect that short-term, likely global $\delta^{34}S$ variations will be superimposed on a longer, first-order trend, defined in part by our data. These nested cycles will track the hierarchical pathways of coupled C–S cycling in the ocean and time varying reservoir sensitivity to changing fluxes, as dictated by sulfate concentration.

ACKNOWLEDGMENTS

We are grateful to L.G. Yang (Administration for the Middle–Upper Proterozoic State-rank Protective Area in Jixian, Tianjin, China) and H.M. Zhang (Tianjin Institute of Geology and Mineral Resource, Tianjin, China) for guiding our field efforts. We are pleased to acknowledge helpful discussions with H. Strauss (Geologisch-Paläontologisches Institut, Westfälische Wilhelms-Universität Münster, Münster, Germany), W.D. Sun (Guangzhou Institute of Geochemistry, Chinese Academy of Sciences, Guangzhou, China), and R.W. Li (Institute of Geology and Geophysics, Chinese Academy of Sciences, Beijing, China). We are grateful for the constructive comments of D. Johnston, G. Shields, and one anonymous reviewer. This research is funded by the Natural Science Foundation of China (Grants 40532012, 40373011, and 49973008), the Chinese Academy of Sciences (Grant KZCX3-SW-141), and U.S. National Science Foundation awards EAR-9725538 and EAR-0207565 for T.W.L.

REFERENCES

Arnold G. L., Anbar A. D., Barling J. and Lyons T. W. (2004) Molybdenum isotope evidence for widespread anoxia in mid-Proterozoic oceans. *Science* **304**, 87–90.

Banner J. L. (1995) Application of the trace element and isotope geochemistry of strontium to studies of carbonate diagenesis. *Sedimentology* **42**, 805–824.

Banner J. L. and Hanson G. N. (1990) Calculation of simultaneous isotopic and trace element variations during water–rock interaction with applications to carbonate diagenesis. *Geochim. Cosmochim. Acta* **54**, 3123–3137.

Bartley J. K., Semikhatov M. A., Kaufman A. J., Knoll A. H., Pope M. C. and Jacobsen S. B. (2001) Global events across the Mesoproterozoic boundary: C and Sr isotopic evidence from Siberia. *Precambrian Res.* **111**, 165–202.

Bartley J. K. and Kah L. C. (2004) Marine carbon reservoir C_{org}-C_{carb} coupling and the evolution of the Proterozoic carbon cycle. *Geology* **32**, 129–132.

Bekker A., Holland H. D., Wang P.-L., Rumble, III, D., Stein H. J., Hannah J. L., Coetzee L. L. and Beukes N. J. (2004) Dating the rise of atmospheric oxygen. *Nature* **427**, 117–120.

Berner R. A. (2001) Modeling atmospheric O_2 over Phanerozoic time. *Geochim. Cosmochim. Acta* **65**, 685–694.

Berner R. A. and Raiswell R. (1983) Burial of organic carbon and pyrite sulfur in sediments over Phanerozoic time: a new theory. *Geochim. Cosmochim. Acta* **47**, 855–862.

Bottomley D. J., Veizer J., Nielsen H. and Moczydlowska M. (1992) Isotopic composition of disseminated sulfur in Precambrian sedimentary rocks. *Geochim. Cosmochim. Acta* **56**, 3311–3322.

Bottrell S. H. and Newton R. J. (2006) Reconstruction of changes in global sulfur cycling from marine sulfate isotopes. *Earth-Sci. Rev.* **75**, 59–83.

Brasier M. D., Shields G., Kuleshov V. N. and Zhegallo L. A. (1996) Integrated chemo- and biostratigraphic calibration of early animal evolution: Neoproterozoic-early Cambrian of southwest Mongolia. *Geol. Mag.* **133**, 445–485.

Brasier M. D. and Lindsay J. F. (1998) A billion years of environmental stability and the emergence of eukaryotes: New data from northern Australia. *Geology* **26**, 555–558.

Brand U. and Veizer J. (1980) Chemical diagenesis of a multicomponent carbonate system −1 Trace elements. *J. Sediment. Petrol.* **50**, 1219–1236.

Buick R., Des Marais D. J. and Knoll A. H. (1995) Stable isotopic compositions of carbonates from the Mesoproterozoic Bangemall Group northwestern Australia. *Chem. Geol.* **123**, 153–171.

Burdett J. W., Arthur M. A. and Richardson M. (1989) A Neogene seawater sulfur isotope age curve from calcareous pelagic microfossils. *Earth Planet. Sci. Lett.* **94**, 189–198.

Busenberg E. and Plummer L. N. (1985) Kinetic and thermodynamic factors controlling the distribution of SO_4 and Na in calcites and selected aragonites. *Geochim. Cosmochim. Acta* **49**, 713–725.

Canfield D. E. (1998) A new model for Proterozoic ocean chemistry. *Nature* **396**, 450–453.

Canfield D. E. (2004) The evolution of the Earth surface sulfur reservoir. *Am. J. Sci.* **304**, 839–861.

Canfield D. E. and Teske A. (1996) Late Proterozoic rise in atmospheric oxygen concentration inferred from phylogenetic and sulphur-isotope studies. *Nature* **382**, 127–132.

Chen J. B., Zhang H. M., Zhu S. X., Zhao Z. and Wang, Z. G. (1980) Research on Sinian Suberathem of Jixian Tianjin (in Chinese). In *Research on Precambrian Geology: Sinian Suberathem in China* (ed. Tianjin Institute of Geology and Mineral Resources, CAGS). Tianjin Sci. & Tech. Press, Tianjin, pp. 56–114.

Chu X., Zhang T., Zhang Q. and Feng L. (2004) Carbon isotopic variations of Proterozoic carbonates in Jixian Tianjin China. *Sci. China (Ser. D)* **47**, 160–170.

Chung F. T. (1977) On the Sinian geochronological scale of China based on isotopic ages for the Sinian strata in the Yenshan Region, North China. *Scientia Sinica* **6**, 818–834.

Claypool G. E., Holser W. T., Kaplan I. R., Sakai H. and Zak I. (1980) The age curves of sulfur and oxygen in marine sulfate and their mutual interpretation. *Chem. Geol.* **28**, 199–260.

Condie K. C. (1998) Episodic continental growth and supercontinents: a mantle avalanche connection. *Earth Planet. Sci. Lett.* **163**, 97–108.

Derry L. A., Kaufman A. J. and Jacobsen S. B. (1992) Sedimentary cycling and environmental change in the late Proterozoic: evidence from stable and radiogenic isotopes. *Geochim. Cosmochim. Acta* **56**, 1317–1329.

Des Marais D. J., Strauss H., Summons R. E. and Hayes J. M. (1992) Carbon isotope evidence for the stepwise oxidation of the Proterozoic environment. *Nature* **359**, 605–609.

Des Marais D. J. (1994) Tectonic control of the crustal organic carbon reservoir during the Precambrian. *Chem. Geol.* **114**, 303–314.

Des Marais D. J. (1997) Isotopic evolution of the biogeochemical carbon cycle during the Proterozoic Eon. *Org. Geochem.* **27**, 185–193.

Des Marais D. J. (2001) Isotopic evolution of the biogeochemical carbon cycle during the Precambrian. In *Stable Isotope Geochemistry*, vol. 43 (eds. J. W. Valley and D. R. Cole). Reviews in Mineralogy & Geochemistry, pp. 555–578.

Farquhar J., Bao H. and Thiemens M. (2000) Atmospheric influence on Earth's earliest sulfur cycle. *Science* **289**, 756–758.

Fike D. A., Grotzinger J. P., Pratt L. M. and Summons R. E. (2006) Oxidation of the Ediacaran ocean. *Nature* **444**, 744–747.

Frank T. D., Lyons T. W. and Lohmann K. C. (1997) Isotopic evidence for the paleoenvironmental evolution of the Mesoproterozoic Helena Formation Belt Supergroup Montana USA. *Geochim. Cosmochim. Acta* **61**, 5023–5041.

Frank T. D., Kah L. C. and Lyons T. W. (2003) Changes in organic matter production and accumulation as a mechanism for isotopic evolution in the Mesoproterozoic ocean. *Geol. Mag.* **140**, 397–420.

Gellatly A. M. and Lyons T. W. (2005) Trace sulfate in mid-Proterozoic carbonates and the sulfur isotope record of biospheric evolution. *Geochim. Cosmochim. Acta* **69**, 3813–3829.

Gill B. C., Lyons T. W. and Saltzman M. R. (2007) Parallel, high-resolution carbon and sulfur isotope records of the evolving Paleozoic marine sulfur reservoir. *Palaeogeog. Palaeoclimat. Palaeoecol.* doi:10.1016/j.palaeo.2007.02.030.

Glesemann A., Jager H. J., Norman A. L., Krouse H. R. and Brand W. A. (1994) On-line sulfur-isotope determination using an elemental analyzer coupled to a mass spectrometer. *Anal. Chem.* **66**, 2816–2819.

Godderis Y. and Veizer J. (2000) Tectonic control of chemical and isotopic composition of ancient oceans: the impact of continental growth. *Am. J. Sci.* **300**, 434–461.

Gorjan P., Veevers J. J. and Walter M. R. (2000) Neoproterozoic sulfur-isotope variation in Australia and global implications. *Precambrian Res.* **100**, 151–179.

Guo J. H., Zhai M. G. and Xu R. H. (2001) Timing of the granulite facies metamorphism in the Sanggan area North China craton: zircon U–Pb geochronology. *Sci. China (Ser. D)* **44**, 1010–1018.

Hofmann H. J. and Chen J. B. (1981) Carbonaceous megafossils from the Precambrian (1800 Ma) near Jixian Northern China. *Can. J. Earth Sci.* **18**, 443–447.

Hoffman P. F. (1991) Did breakout of Laurentia turn Gondwana inside-out? *Science* **252**, 1409–1411.

Hoffman P. F., Kaufman A. J., Halverson G. P. and Schrag D. P. (1998) A Neoproterozoic snowball Earth. *Science* **281**, 1342–1346.

Holland H. D. (2002) Volcanic gases black smokers and the Great Oxidation Event. *Geochim. Cosmochim. Acta* **66**, 3811–3826.

Holser W. T., Schidlowski M., Mackenzie F. T. and Maynard B. J. (1988) Geochemical cycles of carbon and sulfur. In *Chemical Cycles in the Evolution of the Earth* (eds. C. B. Gregor, R. M. Garrels, F. T. Mackenzie and B. J. Maynard). Wiley, New York, p. 276.

Hudson J. D. (1977) Stable isotopes and limestone lithification. *J. Geol. Soc. Lond.* **133**, 637–660.

Hurtgen W. T., Arthur M. A., Suits N. S. and Kaufman A. J. (2002) The sulfur isotopic composition of Neoproterozoic seawater sulfate: implications for a snowball Earth? *Earth Planet. Sci. Lett.* **203**, 413–429.

Hurtgen W. T., Arthur M. A. and Prave A. P. (2004) The sulfur isotope composition of carbonate associated sulfate in Mesoproterozoic to Neoproterozoic carbonates from Death Valley California. *Geol. Soc. Am. Spec. Paper* **379**, 177–194.

Jacobsen S. B. and Kaufman A. J. (1999) The Sr C and O isotopic evolution of Neoproterozoic seawater. *Chem. Geol.* **161**, 37–57.

Jahn B. and Cuvellier H. (1994) Pb–Pb and U–Pb geochronology of carbonate rocks: an assessment. *Chem. Geol.* **115**, 125–151.

Johnston D. T., Wing B. A., Farquhar J., Kaufman A. J., Strauss H., Lyons T. W., Kah L. C. and Canfield D. E. (2005) Active microbial sulfur disproportionation in the Mesoproterozoic. *Science* **310**, 1477–1479.

Kah L. C. and Bartley J. K. (2001) Rodinia and the Mesoproterozoic earth–ocean system. *Precambrian Res.* **111**, 1–3.

Kah L. C., Lyons T. W. and Chesley J. T. (2001) Geochemistry of a 1.2 Ga carbonate-evaporite succession northern Baffin and Bylot Islands: implications for Mesoproterozoic marine evolution. *Precambrian Res.* **111**, 203–234.

Kah L. C., Lyons T. W. and Frank T. D. (2004) Low marine sulphate and protracted oxygenation of the Proterozoic biosphere. *Nature* **431**, 834–838.

Kampschulte A. and Strauss H. (2004) The sulfur isotopic evolution of Phanerozoic seawater based on the analysis of structurally substituted sulfate in carbonates. *Chem. Geol.* **204**, 255–286.

Kao C. S., Hsiung Y. H. and Kao P. (1934) Preliminary notes on Sinian stratigraphy of North China (in Chinese). *Bull. Geol. Soc. China* **13**, 243–276.

Kasting J. F. (1987) Theo retical constraints on oxygen and carbon dioxide concentrations in the Precambrian atmosphere. *Precambrian Res.* **34**, 205–229.

Karhu J. A. and Holland H. D. (1996) Carbon isotopes and the rise in atmospheric oxygen. *Geology* **24**, 867–870.

Kaufman A. J. and Knoll A. H. (1995) Neoproterozoic variations in the C isotopic composition of seawater: stratigraphic and biogeochemical implications. *Precambrian Res.* **73**, 27–49.

Kaufman A. J., Knoll A. H. and Narbonne G. M. (1997) Isotopes ice ages and terminal Proterozoic earth history. *Proc. Natl. Acad. Sci. USA* **94**, 6600–6605.

Knoll A. H. (1992) Biological and biogeochemical preludes to the Ediacaran radiation. In *Origin and Early Evolution of the Metazoa* (eds. J. H. Lipps and P. W. Signor). Plenum, New York, pp. 53–84.

Knoll A. H., Kaufman A. J. and Semikhatov M. A. (1995) The carbon-isotopic composition of Proterozoic carbonates: Riphean successions from northwestern Siberia (Anabar Massif Turukhansk Uplift). *Am. J. Sci.* **295**, 823–850.

Kurtz A. C., Kump L. R., Arthur M. A., Zachos J. C. and Paytan A. (2003) Early Cenozoic decoupling of the global carbon and sulfur cycles. *Paleoceanography* **18**, 1090. doi:10.1029/2003PA000908.

Li H. K., Li H. M. and Lu S. N. (1995) Grain zircon U–Pb ages for volcanic rocks from Tuanshanzi Formation of Changcheng System and their geological implications (in Chinese). *Geochimica* **24**, 43–48.

Li M. R., Wang S. S. and Qiu J. (1996) The ages of glauconites from Tieling and Jingeryu formations Beijing-Tianjin area (in Chinese). *Acta Petrolog. Sinica* **12**, 416–423.

Li R. W., Chen J. S. and Zhang S. K. (1999) Stable carbon and oxygen isotopic compositions of carbonates in middle Mesoproterozoic Wumishan Formation and sea-level change. *Chin. Sci. Bull.* **44**, 2130–2136.

Li R. W., Chen J. S. and Chen Z. M. (2000) Characteristics of the C- and O-isotopic compositions of carbonates in the weathering profile at the unconformable boundary between the early Cambrian and late Proterozoic in Ji County North China (in Chinese with English abstract). *Sci. Geol. Sinica* **35**, 55–59.

Li C., Peng P. A., Sheng G. Y., Fu J. M. and Yan Y. Z. (2003a) A molecular and isotopic geochemical study of Meso- to Neoproterozoic (1.73–0.85 Ga) sediments from the Jixian section Yanshan Basin North China. *Precambrian Res.* **125**, 337–356.

Li R. W., Chen J. S., Zhang S. K. and Chen Z. M. (2003b) Secular variations in carbon isotopic compositions of carbonates from Proterozoic successions in the Ming Tombs Section of the North China Platform. *J. Asian Earth Sci.* **22**, 329–341.

Lindsay J. F. and Brasier M. D. (2000) A carbon isotope reference curve for ca. 1700–1575 Ma McArthur and Mount Isa Basins Northern Australia. *Precambrian Res.* **99**, 271–308.

Lindsay J. F. and Brasier M. D. (2002) Did global tectonic drive early biosphere evolution? Carbon isotope record from 2.6 to 1.9 Ga carbonates of Western Australian basins. *Precambrian Res.* **114**, 1–34.

Lindsay J. F. and Brasier M. D. (2004) The evolution of the Precambrian atmosphere: carbon isotopic evidence from the Australian continent. In *The Precambrian Earth: Tempos and Events (Developments in Precambrian Geology, vol. 12)* (eds. P. G. Eriksson, W. Altermann, D. R. Nelson, W. U. Mueller and O. Catuneau). Elsevier, Amsterdam, pp. 388–403.

Lu S. N. and Li H. M. (1991) A precise U–Pb single zircon age determination for the volcanics of the Dahongyu Formation Changcheng System in Jixian (in Chinese). *Bull. Chin. Acad. Geol. Sci.* **22**, 137–146.

Lu S. N., Yang C. L., Zhu S. X. and Mei H. L. (1996) Precambrian continental crust profile from eastern Hebei to Jixian Tianjin. In *30th IGC Field Trip Guide*, vol. 2 (eds. H. F. Hou and J. S. Zhou). Geological Publishing House, Beijing, pp. T105. 1–T105. 42.

Luepke J. J. and Lyons T. W. (2001) Pre-Rodinian (Mesoproterozoic) supercontinental rifting along the western margin of Laurentia: geochemical evidence from the Belt-Purcell Supergroup. *Precambrian Res.* **111**, 79–90.

Lyons T. W., Kah L. C. and Gellatly A. M. (2004a) The Precambrian sulphur isotope record of evolving atmospheric oxygen. In *The Precambrian Earth: Tempos and Events (Developments in Precambrian Geology, vol. 12)* (eds. P. G. Eriksson, W. Altermann, D. R. Nelson, W. U. Mueller and O. Catuneau). Elsevier, Amsterdam, pp. 421–440.

Lyons T. W., Walter L. M., Gellatly A. M., Martini A. M. and Blake R. E. (2004b) Sites of anomalous organic remineralization in the carbonate sediments of South Florida USA: The sulfur cycle and carbonate-associated sulfate. *Geol. Soc. Am. Spec. Paper* **379**, 161–176.

Lyons T. W., Hurtgen M. T. and Gill B. C. (2005) New insight into the utility of carbonate-associated sulfate. *Geochim. Cosmochim. Acta* **69**, A128.

McCrea J. M. (1950) The isotopic chemistry of carbonates and a paleotemperature scale. *J. Chem. Phys.* **63**, 563–568.

Newton R. J., Pevitt E. L., Wignall P. B. and Bottrell S. H. (2004) Large shifts in the isotopic composition of seawater sulphate across the Permo-Triassic boundary in northern Italy. *Earth Planet. Sci. Lett.* **218**, 331–345.

Page R. W. and Sweet I. P. (1998) Geochronology of basin phases in the western Mt.Isa Inlier and correlation with the McArthur Basin. *Aust. J. Earth Sci.* **45**, 219–232.

Ray J. S., Veizer J. and Davis W. J. (2003) C, O, Sr and Pb isotope systematics of carbonate sequences of the Vindhyan Supergroup India: age diagenesis correlations and implications for global events. *Precambrian Res.* **121**, 103–140.

Rogers J. J. W. and Santosh M. (2002) Configuration of Columbia a Mesoproterozoic supercontinent. *Gondwana Res.* **5**, 5–22.

Schidlowski M. (1989) Evolution of the sulfur cycle in the Precambrian. In *Evolution of the Global Biogeochemical Sulfur Cycle* (eds. P. Brimblecombe and A. Y. Lein). Wiley, New York, pp. 3–19.

Schidlowski M., Eichmann R. and Junge C. E. (1975) Precambrian sedimentary carbonates: carbon and oxygen isotope geochemistry and implications for the terrestrial oxygen budget. *Precambrian Res.* **2**, 1–69.

Seong-Joo L. and Golubic L. (1999) Microfossil populations in the context of synsedimentary micrite deposition and acicular carbonate precipitation: Mesoproterzoic Gaoyuzhuang Formation China. *Precambrian Res.* **96**, 183–208.

Shen Y., Knoll A. H. and Walter M. R. (2003) Evidence for low sulphate and anoxia in a mid-Proterozoic marine basin. *Nature* **423**, 632–635.

Shields G. and Veizer J. (2002) Precambrian marine carbonate isotope database: Version 1.1. *Geochem. Geophys. Geosys.* **3**, U1–U12.

Shields G., Kimura H., Yang J. D. and Gammon P. (2004) Sulphur isotopic evolution of Neoproterozoic-Cambrian seawater: new francolite-bound sulphate δ^{34}S data and a critical appraisal of the existing record. *Chem. Geol.* **204**, 163–182.

Strauss H. (1993) The sulfur isotopic record of Precambrian sulfates: new data and a critical evaluation of the existing record. *Precambrian Res.* **63**, 225–246.

Strauss H. (1997) The isotopic composition of sedimentary sulfur through time. *Palaeogeog. Palaeoclimat. Palaeoecol.* **132**, 97–118.

Strauss H. (1999) Geological evolution from isotope proxy signals—sulfur. *Chem. Geol.* **161**, 89–101.

Strauss H. (2002) The isotopic composition of Precambrian sulphides-seawater chemistry and biological evolution. *Spec. Publs. Int. Ass. Sediment.* **33**, 67–105.

Takano B. (1985) Geochemical implications of sulfate in sedimentary carbonates. *Chem. Geol.* **49**, 393–403.

Ueda A., Cameron E. M. and Krouse H. R. (1990) ^{34}S-enriched sulphate in the Belcher Group, N.W.T. Canada: evidence for dissimilatory sulphate reduction in the early Proterozoic ocean. *Precambrian Res.* **49**, 229–233.

Walker J. C. G., Klein C., Schidlowski M., Schopf J. W., Stevenson D. J. and Walter M. R. (1983) Environmental evolution of the Archean-Early Proterozoic earth. In *Earth's Earliest Biosphere: Its Origin and Evolution* (ed. J. W. Schopf). Princeton University Press, Princeton, pp. 263–289.

Walter M. R. and Veevers J. J. (1997) Australian Neoproterozoic palaeogeography, tectonics and supercontinental connections. *AGSO J. Austr. Geol. Geophys.* **17**, 73–92.

Walter M. R., Veevers J. J., Calver C. R., Gorjan P. and Hill A. C. (2000) Dating the 840–544 Ma Neoproterozoic interval by isotopes of strontium, carbon, and sulfur in seawater, and some interpretative models. *Precambrian Res.* **100**, 371–433.

Wan Y. S., Zhang Q. D. and Song T. R. (2003) SHRIMP ages of detrital zircons from the Changcheng System in the Ming Tombs area Beijing: Constraints on the protolith nature and maximum depositional age of the Mesoproterozoic cover of the North China Craton. *Chin. Sci. Bull.* **48**, 2500–2506.

Wang H. (1985) *Atlas of the Palaeogeography of China*, 143 pp. Cartogaphic Publishing House, Beijing.

Wang H. Z. and Qiao X. F. (1987) Proterozoic geotectonic units of China and the nature of their boundaries (in Chinese). *Precambrian Geol.* **3**, 1–14.

Wang K. F. and Chen J. S. (1993) Constraints on the stable isotopic composition of sedimentary carbonates from the Tieling Formation in the Yanshan region (in Chinese). *Geochimica* **1**, 10–17.

Wang S., Sang H., Qiu J., Chen M. and Li M. (1995) The forming ages of Yangzhuang and Wumishan formations in Jixian section, northern China (in Chinese). *Sci. Geol. Sinica* **30**, 166–173.

Xiao S., Knoll A. H., Kaufman A. J., Yin L. and Zhang Y. (1997) Neoproterozoic fossils in Mesoproterozoic rocks? Chemostratigraphic resolution of a biostratigraphic conundrum from the North China Platform. *Precambrian Res.* **84**, 197–220.

Yale L. B. and Carpenter S. J. (1998) Large igneous provinces and giant dike swarms: proxies for supercontinental cyclicity and mantle convection. *Earth Planet. Sci. Lett.* **163**, 109–122.

Yanagisawa H. and Sakai H. (1983) Thermal decomposition of barium sulfate-vanadium pentaoxide-silica glass mixtures for preparation of sulfur dioxide in sulfur isotope ratio measurements. *Anal. Chem.* **55**, 985–987.

Zhai M. G., Bian A. G. and Zhao T. P. (2000) The amalgamation of the supercontinent of North China Craton at the end of Neo-Archaean and its breakup during late Palaeoproterozoic and Meso-Proterozoic. *Sci. China (Ser. D)* **43**(suppl.), 219–232.

Zhao Z. (1995) Characteristics of Proterzoic carbonate rocks in Jixian by means of oxygen and carbon isotope composition (in Chinese). *Acta Sedimentol. Sinica* **13**, 46–53.

Zhao C. L., Li R. F. and Zhou J. S. (1997) *Sedimentology and Petroleum Geology of the Meso- and Neo-Proterozoic in North China* (in Chinese with English abstract), 253 pp. Geological Publishing House, Beijing.

Zhao G. C., Cawood P. A., Wilde S. A. and Sun M. (2002) Review of global 2.1–1.8 Ga orogens: implications for a pre-Rodinia supercontinent. *Earth-Sci. Rev.* **59**, 125–162.

Zhao G. C., Sun M. and Wilde S. A. (2003) Major tectonic units of the North China Craton and their Paleoproterozoic assembly. *Sci. China (Ser. D)* **46**, 23–38.

Zhao G. C., Sun M., Wilde S. A. and Li S. Z. (2004) Paleo-Mesoproterozoic supercontinent: assembly growth and breakup. *Earth-Sci. Rev.* **67**, 91–123.

Zhong H. and Chen J. (1992) Carbon isotope evidence for lower biomass about 1400 Ma ago (in Chinese). *Sci. Geol. Sinica* **27**, 160–168.

Zhu S. and Chen H. (1995) Megascopic multicellular organisms from the1700-Million-year-old Tuanshanzi Formation in the Jixian area North China. *Science* **270**, 620–622.

Zhu S. X., Sun S. F., Huang X. G., He Y. Z., Zhu G. X., Sun L. X. and Zhang K. (2000) Discovery of carbonaceous compressions and their multicellular tissues from the Changzhougou Formation (1800 Ma) in the Yanshan Range North China. *Chin. Sci. Bull.* **45**, 841–847.

Associate editor: Graham A. Logan